Endogenous Glucocorticoid Signaling Regulates CD8+ T Cell Differentiation and Development of Dysfunction in the Tumor Microenvironment

As Published: 10.1016/J.IMMUNI.2020.08.005

Publisher: Elsevier BV

Persistent URL: https://hdl.handle.net/1721.1/133832

Version: Author's final manuscript: final author's manuscript post peer review, without publisher's formatting or copy editing

Published in final edited form as:

Immunity. 2020 September 15; 53(3): 658–671.e6. doi:10.1016/j.immuni.2020.08.005.

Endogenous glucocorticoid signaling regulates effector differentiation and development of dysfunction in CD8+ T cells in the tumor microenvironment

Nandini Acharya[1,9], **Asaf Madi**[1,2,9], **Huiyuan Zhang**[1], **Max Klapholz**[1], **Giulia Escobar**[1], **Shai Dulberg**[2], **Elena Christian**[1,3], **Michelle Ferreira**[4], **Karen O. Dixon**[1], **Geoffrey Fell**[5], **Katherine Tooley**[1], **Davide Mangani**[1], **Junrong Xia**[1], **Meromit Singer**[3,6,7], **Marcus Bosenberg**[4], **Donna Neuberg**[5], **Orit Rozenblatt-Rosen**[3], **Aviv Regev**[3,8,*], **Vijay K. Kuchroo**[1,*], **Ana C. Anderson**[1,10,*]

[1]Evergrande Center for Immunologic Diseases and Ann Romney Center for Neurologic Diseases, Harvard Medical School and Brigham and Women's Hospital, Boston, MA, 02115

[2]Department of Pathology, Sackler School of Medicine, Tel Aviv University, Tel Aviv, Israel

[3]Klarman Cell Observatory, Broad Institute of MIT and Harvard, Cambridge, MA 02142

[4]Departments of Dermatology, Pathology, and Immunobiology, Yale University School of Medicine, New Haven, CT 06510

[5]Department of Data Sciences, Dana-Farber Cancer Institute, Boston, MA 01225

[6]Department of Immunology, Harvard Medical School, Boston, MA 02115

[7]Department of Biostatistics and Computational Biology, Dana-Farber Cancer Institute, Boston, MA, 02115

[*]Correspondence: vkuchroo@evergrande.hms.harvard.edu (V.K.K.), aregev@broadinstitute.org (A.R.), acanderson@bwh.harvard.edu (A.C.A).

Authors Contributions

Conceptualization: N.A., A. M., A.C.A

Methodology: N.A., A.M., A.C.A., and A.R.

Investigation: N.A., A.M.

Formal analysis: N.A., A.M., S.D., M.S., G.F. and D. N.

Resources: H.Z., M.K., G.E., M.F., J.X., E.C., K.O.D, K.T., D.M., M.B

Writing: N.A., A.M., A.C.A., V.K.K., and A.R.

Supervision: O.R.R., A.C.A., V.K.K., and A. R.

Funding acquisition: A.C.A., V.K.K., and A.R.

Declaration of interests

A.C.A. is a member of the SAB for Tizona Therapeutics, Compass Therapeutics, Zumutor Biologics, and Astellas Global Pharma Development Inc., which have interests in cancer immunotherapy. V.K.K. is a member of the SAB for Astellas Global Pharma Development Inc., and has an ownership interest and is a member of the SAB for Tizona Therapeutics. A.R. and V.K.K. are co-founders of and have an ownership interest in Celsius Therapeutics. A.C.A.'s and V.K.K.'s interests were reviewed and managed by the Brigham and Women's Hospital and Partners Healthcare in accordance with their conflict of interest policies. M. B. is a consultant for Eli Lilly and Company. A.R. is also SAB member for Thermo Fisher, Neogene Therapeutics, Asimov, and Syros Pharmaceuticals, and an equity holder in Immunitas. A.R.'s interests were reviewed and managed by the Broad Institute and HHMI in accordance with their conflict of interest policies. A provisional patent application was filed including work in this manuscript.

[8]Howard Hughes Medical Institute, Department of Biology, Koch Institute and Ludwig Center, Massachusetts Institute of Technology, Cambridge, MA 02142

[9]These authors contributed equally

[10]Lead Contact

Abstract

Identifying signals in the tumor microenvironment (TME) that shape $CD8^+$ T cell phenotype can inform novel therapeutic approaches for cancer. Here, we identified a gradient of increasing glucocorticoid receptor (GR) expression and signaling from naive to dysfunctional $CD8^+$ tumor-infiltrating lymphocytes (TILs). Conditional deletion of the GR in $CD8^+$ TILs improved effector differentiation, reduced expression of the transcription factor TCF-1, and inhibited the dysfunctional phenotype, culminating in tumor growth inhibition. GR signaling transactivated the expression of multiple checkpoint receptors and promoted the induction of dysfunction-associated genes upon T cell activation. In the TME, monocyte-macrophage lineage cells produced glucocorticoids and genetic ablation of steroidogenesis in these cells as well as localized pharmacologic inhibition of glucocorticoid biosynthesis improved tumor growth control. Active glucocorticoid signaling associated with failure to respond to checkpoint blockade in both pre-clinical models and melanoma patients. Thus, endogenous steroid hormone signaling in $CD8^+$ TILs promotes dysfunction, with important implications for cancer immunotherapy.

eTOC (In brief)

Acharya *et al.* uncover a gradient of increasing glucocorticoid signaling from naïve to dysfunctional $CD8^+$ tumor-infiltrating lymphocytes. This gradient regulates effector transition and development of dysfunction. Glucocorticoid is produced locally by tumor-associated monocyte-macrophage lineage cells and presence of active glucocorticoid signaling associates with poor response to immune checkpoint blockade.

Graphical Abstract

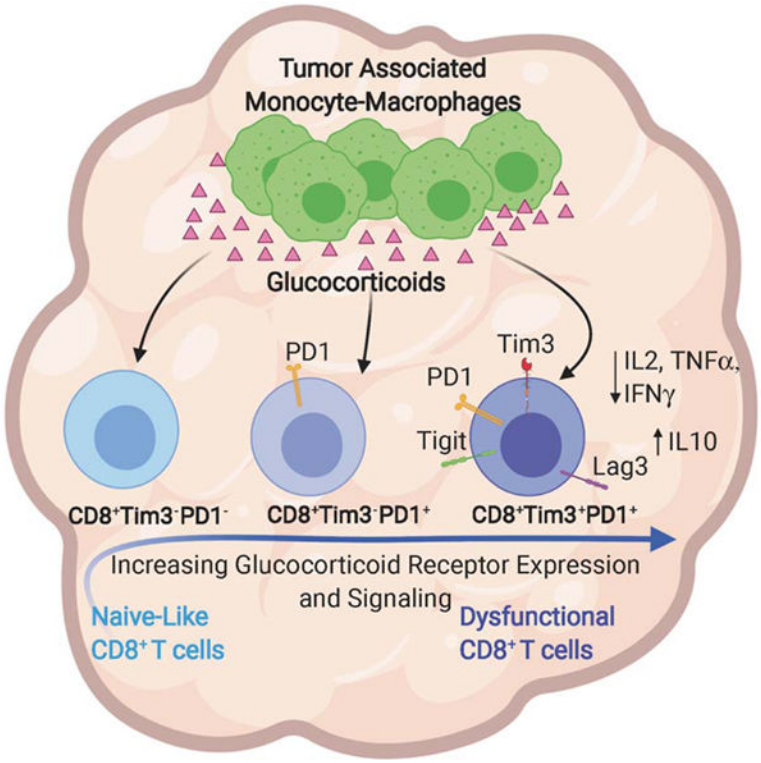

Keywords

CD8$^+$ T cell; cancer; dysfunction; exhaustion; glucocorticoid; *Nr3c1*; TCF-1; steroid

Introduction

Although the immune system has the capacity to fight cancer, signals present within the tumor microenvironment (TME) actively suppress anti-tumor immune responses. In particular, CD8$^+$ T cells, key mediators of anti-tumor immunity, undergo altered effector differentiation that culminates in the development of a dysfunctional or “exhausted” state (Danilo et al., 2018; Wherry and Kurachi, 2015). Dysfunctional CD8$^+$ T cells exhibit defective cytotoxicity, pro-inflammatory cytokine production, and induction of the immunosuppressive cytokine interleukin (IL)-10 (Jin et al., 2010). Thus, dysfunctional CD8$^+$ T cells are not only poor mediators of tumor clearance but can also contribute to immunosuppression in the TME. Therefore, understanding the T cell intrinsic and extrinsic signals that contribute to the development of dysfunction is of key importance in devising effective therapies to improve anti-tumor CD8$^+$ T cell responses.

Glucocorticoids (GCs) are steroid hormones derived from the metabolic breakdown of cholesterol. The GR resides in the cytosol in its inactive state and translocates to the nucleus upon binding to GC. In the nucleus, the GR can regulate gene expression either directly (trans-activation) or indirectly (trans-repression) by affecting the binding of other transcription factors (TFs) to the promoter regions of their respective targets (Oakley and Cidlowski, 2013). GCs suppress a number of inflammatory indices and have been used since

the 1950s for treating excessive inflammation in patients with asthma and autoimmune diseases. Currently, GCs are routinely used to manage excessive inflammation in cancer patients treated with immune checkpoint blockade(ICB) (Kumar et al., 2017).

Despite their widespread use, surprisingly little is known regarding the molecular circuitry by which GCs suppress immune responses (Cain and Cidlowski, 2017; Munck et al., 1984). The prevailing dogma attributes the anti-inflammatory effects of GCs to transrepression, whereby the GR interferes with the function of TFs that have key roles in driving pro-inflammatory responses, such as AP-1 (Jonat et al., 1990; Yang-Yen et al., 1990) and NF-κB (Auphan et al., 1995; Rhen and Cidlowski, 2005; Scheinman et al., 1995; Smoak and Cidlowski, 2004). However, GCs have also been associated with enhanced expression of IL-10 (Barrat et al., 2002), raising the possibility that in addition to actively repressing pro-inflammatory gene expression, they may also promote suppression via transactivation of immune-suppressive genes.

Here, we examined whether GC signaling had a role in shaping anti-tumor $CD8^+$ T cell responses. From our analyses of the RNA profiles of $CD8^+$ tumor-infiltrating (TIL) populations that exhibit distinct effector capacities and are identified by their pattern of Tim-3 and PD-1 checkpoint receptor expression (Sakuishi et al., 2010; Singer et al., 2016), we identified *Nr3c1*, the gene encoding the glucocorticoid receptor (GR), as being most highly expressed in terminally dysfunctional Tim-3^+PD-1^+ $CD8^+$ TILs. Accordingly, we identified a gradient of increasing GC signaling from naïve to dysfunctional $CD8^+$ TILs. GR-deficient $CD8^+$ TILs exhibited reduced expression of TCF-1, improved effector differentiation and function, but failed to develop dysfunctional phenotype, resulting in tumor growth inhibition. The GR promoted dysfunctional phenotype by transactivating the expression of multiple checkpoint receptors together with IL-10 and inducing multiple T cell dysfunction genes. We further found that monocyte-macrophage lineage cells were a chief source of GC within the TME, and that the presence of active GC signaling correlated with failure to respond to checkpoint blockade in both pre-clinical tumor models and melanoma patients. Our findings highlight a role for endogenous steroid hormone signaling in $CD8^+$ TILs in non-hormonally driven cancers with important implications for the application of ICB therapy.

Results

A gradient of glucocorticoid signaling in $CD8^+$ TILs

Analysis of RNA profiles (Singer et al., 2016), showed that *Nr3c1,* the gene encoding the glucocorticoid receptor (GR), is most highly expressed in the Tim-3^-PD-1^+ $CD8^+$ and Tim-3^+PD-1^+ $CD8^+$TIL subsets that contain effector and terminal dysfunctional $CD8^+$ TILs, respectively (Figure S1A). Indeed, examination of GR protein showed a gradient of increasing expression across $CD8^+$ TILs with highest expression in Tim-3^+PD-1^+ $CD8^+$TILs in two different tumor models, MC38-Ova^{dim} colon carcinoma and B16F10 melanoma (Figure 1A and S1B). Further examination showed higher GR expression in tumor-antigen specific (Ova) $CD8^+$ TILs (Figure 1B), indicating increased GR signaling upon TCR engagement. Consistent with the expression pattern on murine $CD8^+$ TILs, the GR was also most highly expressed in Tim-3^+PD-1^+ $CD8^+$ TILs from human colon carcinoma tumors

(Figure 1C). Together these data indicated a gradient of increasing GR signaling from naive to terminally dysfunctional $CD8^+$ TILs subsets.

To confirm this, we scored the expression of a previously established GC signature (Phuc Le et al., 2005) in the single-cell RNA-Seq (scRNA-Seq) profiles of $CD8^+$ TILs (Star Methods) (Singer et al., 2016) from B16F10 melanoma and observed a gradient of low- to high-expressing cells (Figures 1D, panel I and S1C). Low GC signature-expressing cells expressed high levels of genes associated with naïve T cells (*Ccr7, Tcf7),* while intermediate and high GC signature-expressing cells expressed high levels of effector (*Tbx21, Gzmb*) and dysfunction genes (*Entpd1, Tox)*, respectively (Figure S1D). Of note, cells with high expression of the GC signature also expressed *Mt1* and *Nfil3*, known GR target genes (Karin and Herschman, 1979) (Carey et al., 2013) that we have previously implicated in T cell dysfunction (Singer et al., 2016; Zhu et al., 2015) (Figure S1E). These data indicated that naïve and dysfunctional $CD8^+$ TILs mark the spectrum of low to high GC signature-expressing cells, respectively. Indeed, scoring of all of the cells for expression of the GC, naïve, and dysfunction signatures showed that as $CD8^+$ TILs acquire high expression of the GC signature they transition from the naïve to the dysfunctional T cell state (Figure 1D, **panels II-IV**). We further scored the GC signature on the scRNA-Seq profiles of $CD8^+$ T cells from chronic LCMV infection (Chen et al., 2019). Consistent with our observations in $CD8^+$ TILs, we found that many of the cells that scored highly for expression of the GC signature also scored highly for the dysfunction signature (Figure S1F). Collectively, these data indicated that increasing GC signaling was associated with loss of effector function and acquisition of dysfunctional phenotype in $CD8^+$ T cells.

Glucocorticoid signaling dampens effector phenotype and promotes features of dysfunction in $CD8^+$ T cells

Accordingly, we hypothesized that GC signaling might promote T cell dysfunction. We tested the effect of repeated activation of $CD8^+$ T cells in the presence of synthetic GC (dexamethasone; Dex) *in vitro*. In line with observations in acutely activated cells (Barrat et al., 2002; Bianchi et al., 2000; Brattsand and Linden, 1996; Rhen and Cidlowski, 2005), we found that repeated activation in the presence of GC profoundly suppressed the production of the pro-inflammatory cytokines IL-2, TNF- α, and IFN-γ, and induced the immune-suppressive cytokine IL-10 (Figure 2A), a phenotype consistent with dampened effector function. Additionally, we found that GC treatment dramatically induced checkpoint receptors, including PD-1, Tim-3, and Lag-3, but not Tigit (Figure 2B). Notably, the GC-mediated induction of checkpoint receptor expression was conserved in human $CD8^+$ T cells (Figure 2C). Additionally, we observed that GC increased the frequency of Tim-3^+PD-1^+ $CD8^+$ T cells in both murine and human samples (Figure S2A,B). The observed effects of GC were not due to reduced T cell survival or altered proliferation (Figure S2C,D). We further tested the effect of the natural GC, corticosterone, on the expression of checkpoint receptors and found that it recapitulated the effects of Dex (Figure S2E).

The observed effects of GC on $CD8^+$ T cells depended on *Nr3c1*. We found that *Nr3c2*, which encodes the mineralocorticoid receptor (MR) that shares high structural homology with GR and can bind GCs with high affinity (Arriza et al., 1987) is not expressed by wild

type (WT) $CD4^+$ and $CD8^+$ T cells or in $CD8^+$ T cells from mice that lack *Nr3c1* expression specifically in mature $CD8^+$ T cells (E8i-Cre^+ *Nr3c1*$^{fl/fl}$) (Figure S2F). Further, comparison of the RNA profiles of WT (E8i-Cre^- *Nr3c1*$^{fl/fl}$) and E8i-Cre^+ *Nr3c1*$^{fl/fl}$ $CD8^+$ T cells stimulated with or without GC showed distinct GC-induced changes in WT but not E8i-Cre^+ *Nr3c1*$^{fl/fl}$ $CD8^+$ T cells, indicating that GC-induced transcription in $CD8^+$ T cells was *Nr3c1* dependent (Figure S2G). Thus, repeated stimulation in the presence of active GC signaling dramatically influenced the effector differentiation of $CD8^+$ T cells, resulting in cells that exhibited features shared with dysfunctional T cells, including expression of multiple checkpoint receptors, dampened pro-inflammatory cytokine production, and increased IL-10 production.

We next tested whether GC signaling impacted the functional state of $CD8^+$ TILs *in vivo* using E8i-Cre^+ *Nr3c1*$^{fl/fl}$ mice. Examination of T cell development and the steady state peripheral immune compartment of these mice showed no gross differences compared to WT littermate controls (Figures S3A–D). We further confirmed that the deletion of *N3rc1* was specific to $CD8^+$ T cells (Figure S3E). We implanted either MC38-Ova^{dim} or B16F10 melanoma cells into WT and E8i-Cre^+ *Nr3c1*$^{fl/fl}$ mice and found that E8i-Cre^+ *Nr3c1*$^{fl/fl}$ mice exhibited improved tumor growth control in both models (Figures 3A and S4A), indicating that the effect of GC signaling in $CD8^+$ T cells was conserved across tumor types.

We next examined how loss of GC signaling impacted the differentiation and function of $CD8^+$ TILs by examining $CD8^+$ TILs at the early (when tumor sizes were not significantly different across the two groups) and intermediate stages of tumor progression. At both stages, there were no significant differences in the frequency of H-2K^b-OVA$_{257–264}$ dextramer$^+$ $CD8^+$ TILs between the WT and the E8i-Cre^+ *Nr3c1*$^{fl/fl}$ mice (Figure 3B). However, the $CD8^+$ TILs from E8i-Cre^+ *Nr3c1*$^{fl/fl}$ mice exhibited enhanced responses to tumor-antigen (OVA$_{257–264}$), as well as polyclonal stimulation, producing more IL-2, TNF-α, and IFN-γ (Figure 3C and S4B). Indeed, the $CD8^+$ TILs from E8i-Cre^+ *Nr3c1*$^{fl/fl}$ mice were more polyfunctional in terms of pro-inflammatory cytokine production (Figure S4C). $CD8^+$ TILs from E8i-Cre^+ *Nr3c1*$^{fl/fl}$ mice further exhibited higher cytotoxic capacity, as shown by the increased frequency of Granzyme $B^+CD107a^+$ cells upon OVA$_{257–264}$ stimulation at both stages (Figure 3D). We examined IL-10 production and found that although at the early stage there were no significant differences, at the intermediate stage the $CD8^+$ TILs from E8i-Cre^+ *Nr3c1*$^{fl/fl}$ mice produced lower amounts of IL-10 (Figure 3E and S4D). As our data indicated that $CD8^+$ TILs from E8i-Cre^+ *Nr3c1*$^{fl/fl}$ mice exhibited increased effector function, we examined expression of the transcription factor TCF-1, which is known to play a critical role in regulating effector T cell differentiation (Danilo et al., 2018; Tiemessen et al., 2014) and whose expression has been reported to be modulated by *Nr3c1* (Yu et al., 2017). At both stages, we found that the lack of GR resulted in reduced expression of TCF-1 in tumor-antigen specific $CD8^+$ TILs (Figure 3F). Lastly, we examined the expression of checkpoint receptors. At the early stage, we observed low Tim-3 and PD-1 expression, which did not differ between genotypes; however, at the intermediate stage, we observed that not only was there a dramatic reduction in the frequency of $CD8^+$ TILs co-expressing PD-1, Tim-3, Lag-3, and Tigit in $CD8^+$ TILs from E8i-Cre^+ *Nr3c1*$^{fl/fl}$ mice (Figure 3G), but also the expression level of each of these checkpoint receptors was significantly reduced (Figure S4E). Of note, Tigit expression was suppressed in $CD8^+$ TILs

from E8i-Cre^{+} *Nr3c1*$^{fl/fl}$ mice (Figure 3G and S4E), in contrast to our *in vitro* observations where Tigit expression was not induced by GR stimulation (Figure 2B). Furthermore, the few Tim-3^{+}PD-1^{+}CD8^{+} TILs in E8i-Cre^{+} *Nr3c1*$^{fl/fl}$ mice exhibited increased pro-inflammatory cytokine production in response to $OVA_{257–264}$ stimulation (Figure S4F), in contrast to their typical terminally dysfunctional phenotype observed in WT mice. These observations were not due to increased recruitment or proliferation of CD8^{+} T cells in E8i-Cre^{+} *Nr3c1*$^{fl/fl}$ mice as we observed no significant differences in either the expression of Ki-67 or the absolute number of the CD8^{+} TILs in WT and E8i-Cre x *Nr3c1*$^{fl/fl}$ mice (Figures S4G and H).

Importantly, the effects of the loss of *Nr3c1* in CD8^{+} TILs were cell intrinsic. Checkpoint receptor expression on CD4^{+} TILs in E8i-Cre^{+} *Nr3c1*$^{fl/fl}$ mice was not significantly different from that of WT CD4^{+} TILs (Figures S4I and J). Further, when congenically marked CD8^{+} T cells from WT and E8i-Cre^{+} *Nr3c1*$^{fl/fl}$ mice were co-transferred into Rag$^{-/-}$ recipient mice followed by implantation of MC38-Ova^{dim} tumors, only the CD8^{+} TILs from E8i-Cre^{+} *Nr3c1*$^{fl/fl}$ mice exhibited increased expression of pro-inflammatory cytokines and cytotoxic capacity concomitant with reduced expression of PD-1 and Tim-3 (Figure 3H). Collectively, these data indicated that GC signaling acted cell intrinsically to shape effector differentiation and development of dysfunction in CD8^{+} TILs.

Glucocorticoid signaling transactivates checkpoint receptor expression and IL-10 and induces T cell dysfunction genes

Our *in vivo* data indicated a relationship between *Nr3c1* and expression of checkpoint receptors and IL-10 in murine colon cancer. In line with this, a previous study implicated GC in promoting PD-1 expression on T cells (Xing et al., 2015), although the underlying mechanism was not examined. We further found a strong positive correlation of *NR3C1* mRNA levels with *HAVCR2* (Tim-3), *PDCD1* (PD-1), *LAG3*, *TIGIT* and *IL10* mRNA levels in human colon adenocarcinoma from TCGA (http://cancergenome.nih.gov/) (Figure S5A). We therefore tested if the GR directly regulated the expression of checkpoint receptor and IL-10. First, we analyzed GR-binding peaks in the loci of *Havcr2* (Tim-3), *Pdcd1* (PD-1), *Lag3*, *Tigit,* and *IL10* in publicly available ChIP-seq data (Oh et al., 2017) from bone marrow-derived macrophages (BMDMs). We found GR-binding peaks in the loci of *Havcr2, Lag3*, and *IL10* but not *Pdcd1* or *Tigit*, likely reflecting the lack of PD-1 and Tigit expression in BMDMs (Figure S5B–F). Of note, some of the GR binding peaks in the *Havcr2, Lag3*, and *IL10* loci overlapped with regions of accessible chromatin in dysfunctional CD8^{+} TILs (Philip et al., 2017), which are known to express these checkpoint receptors as well as IL-10 (Figure S5B–F). We therefore tested the effect of GR binding to the *cis*-regulatory elements in the loci of *Havcr2*, *Pdcd1*, *Lag3*, and *Tigit* using luciferase reporter assays. For *IL10*, we utilized luciferase reporters of a previously established enhancer element of *Il10* – HSS^{+}2.98 as well as the proximal promoter (−1.5kb)(Karwacz et al., 2017). We transfected the different luciferase reporter constructs along with a *Nr3c1* expressing vector or empty control vector into 293T cells and treated the cells with GC to assay the transactivation capability of the GR. In line with our observations in GC-treated CD8^{+} T cells (Figure 2), the GR potently transactivated Tim-3, PD-1, Lag-3, and IL-10 expression (Figure 4A–C and E). Tigit was also induced but to a much lower degree (Figure

4D). Given that the GR could transactivate checkpoint receptors and IL10, we hypothesized that the GR could also potentially drive the expression of genes associated with $CD8^+$ T cell dysfunction. To test this, we analyzed the RNA profiles from $CD8^+$ T cells undergoing repeated stimulation in the presence of GC or vehicle control. We found that 463 GC-induced genes overlapped with the T cell dysfunction signature (Table S1). The genes induced by GC treatment significantly ($p=9.4\times10^{-52}$, Mean-rank Gene Set Test) overlapped with the genes expressed by terminally dysfunctional $Tim3^+PD1^+$ $CD8^+$ TILs while the genes suppressed by GC significantly ($p=1.4\times10^{-26,}$ Mean-rank Gene Set Test) overlapped with the genes expressed by the $Tim3^-PD1^-CD8^+$ T cells that exhibit effector capacity (Figure 4F and S5G).

Myeloid cells are the primary source of glucocorticoid in the TME

Although steroids are mainly synthesized in the adrenal cortex, it has been suggested that tumor cells are capable of extra-adrenal steroidogenesis (Sidler et al., 2011). Accordingly, we asked whether local sources in the TME provided endogenous GC. Steroids are produced by the enzymatic breakdown of cholesterol, where cytochrome P450 cholesterol side-chain cleavage enzyme (Cyp11a1) catalyzes the first and the rate-limiting step that breakdowns cholesterol to pregnenolone, the precursor of all steroid hormones (Payne and Hales, 2004). We quantified pregnenolone levels in the tumor tissue and spleen of MC38-Ova^{dim} tumor-bearing and tumor-free mice and found a high level of pregnenolone in the tumor tissue while levels in the spleen of tumor- and non-tumor-bearing mice did not differ (Figure 5A). These data indicated that steroids may be produced locally in the TME. We next examined which cell types might be responsible for steroid production in the TME by examining expression of Cyp11a1. We found that neither *in vitro* cultured nor *ex vivo* isolated MC38-Ova^{dim} cells expressed Cyp11a1 (Figure 5B). Examination of other cells in the TME showed that cancer-associated fibroblasts (CAFs) ($CD45^-GFP^-PDGFR\alpha^+$), tumor-associated dendritic cells (TADCs), and T cells (mostly $CD4^+$ T cells) expressed Cyp11a1 but at much lower levels compared to tumor-associated monocyte-macrophage lineage cells (Figure 5B). To study the relevance of steroid production from monocyte-macrophage lineage cells on tumor growth, we implanted MC38-Ova^{dim} tumor cells in WT ($LysMCre^-$ $Cyp11a1^{fl/fl}$) and $LysMCre^+$ $Cyp11a1^{fl/fl}$ mice and observed significant tumor growth control in $LysMCre^+$ $Cyp11a1^{fl/fl}$ mice (Figure 5C). We next examined the differentiation and function of $CD8^+$ TILs from WT and $LysMCre^+$ $Cyp11a1^{fl/fl}$ mice at an early stage of tumor progression when tumor sizes were not significantly different across groups. We found no significant difference in the frequency of H-$2K^b$-$OVA_{257–264}$ $dextramer^+$ $CD8^+$ TILs; however, the $CD8^+$ TILs from $LysMCre^+$ $Cyp11a1^{fl/fl}$ mice produced more pro-inflammatory cytokines and had increased cytotoxic capacity (Figure 5D). Further, the $CD8^+$ TILs from $LysMCre^+$ $Cyp11a1^{fl/fl}$ mice had a reduced frequency of $TCF\text{-}1^+$ tumor-antigen specific cells and checkpoint receptor-expressing cells (Figure 5D). Thus, the observed phenotype of $CD8^+$ TILs from $LysMCre^+$ $Cyp11a1^{fl/fl}$ resembled that observed in E8i-Cre^+ $Nr3c1^{fl/fl}$ mice (Figure 3 and S4).

We next examined whether GC was indeed produced in tumor tissue. In line with our observations of pregnenolone production (Figure 5A), we found that corticosterone was produced at high levels in the tumor tissue whereas the levels present in the spleen of tumor-

and non-tumor-bearing mice did not differ (Figure 5E). Further, tumor explants cultured in the presence of Metyrapone, an inhibitor of GC synthesis, produced less corticosterone (Figure S6A). Together these data indicated local GC production in the TME. Given our data indicating a key role for steroid production by tumor-associated monocyte-macrophage lineage cells, we examined corticosterone production in the tumor and spleen of WT and LysMCre^{+} *Cyp11a1*$^{fl/fl}$ mice and found significantly reduced corticosterone production in the tumor but not in the spleen (Figure S6B). Intra-tumoral administration of corticosterone to LysMCre^{+} *Cyp11a1*$^{fl/fl}$ mice abrogated the previously observed control of tumor progression (Figure S6C), further pointing to monocyte-macrophage lineage-derived GC as a key determinant of anti-tumor immunity.

To confirm that tumor-associated monocyte-macrophage lineage cells were indeed capable of GC production, we examined their expression of the enzymes involved in canonical GC biosynthesis (StAR,Cyp21a1,Cyp17a1,Cyp11b1,Hsd3b1). We found that they expressed all enzymes to varying degrees with the exception of Hsd3b1 (Figure S6D). We therefore tested the expression of other Hsd3b isoforms (Hsd3b3, Hsd3b6) that are capable of steroid biosynthesis and have been reported in mice (Abbaszade et al., 1995; Clarke et al., 1993). We found expression of Hsd3b3 but not Hsd3b6 (Figure S6D), consistent with previous reports indicating that Hsd3b1 is expressed mainly in the adrenal glands and gonads whereas other steroidogenic tissues express Hsd3b3 (Bain et al., 1991). We further confirmed that tumor-associated monocyte-macrophage lineage cells could produce GC as their production of corticosterone *ex vivo* was significantly inhibited by Metyrapone (Figure 5F). Lastly, we administered Metyrapone intra-tumorally to MC38-Ova^{dim} tumor-bearing mice and observed dramatic tumor growth inhibition (Figure 5G). We analyzed the CD8^{+} TILs from Metyrapone-treated mice at an early stage of tumor progression, when tumor sizes were not significantly different across groups, and found that their functional properties resembled that of CD8^{+} TILs from E8i-Cre^{+} *Nr3c1*$^{fl/fl}$ mice and LysM-Cre^{+} *Cyp11a1*$^{fl/fl}$ mice (Figure 5H). Collectively, these data indicated that tumor-associated monocyte-macrophage lineage cells were the chief source of GC that shaped anti-tumor effector CD8^{+} T cell responses in the TME.

Glucocorticoid signaling in CD8^{+} T cells affects responses to immunotherapy

Our data indicated that steroid signaling in the TME was a key determinant of anti-tumor immunity in murine colon carcinoma. We therefore examined whether steroid abundance impacted on disease outcome in human gastrointestinal cancers. We found that low *Cyp11a1* mRNA levels were associated with a substantial survival benefit in patients with colon adenocarcinoma and stomach adenocarcinoma (Figure 6A). Next, we tested whether steroid signaling affected the response to ICB. We treated WT and E8i-Cre^{+} *Nr3c1*$^{fl/fl}$ mice bearing MC38-Ova^{dim} tumors with anti-PD1 and found that the loss of GC signaling in CD8^{+} T cells dramatically improved the response to anti-PD-1 (Figure 6B). Conversely, we found that administration of high-dose GC abrogated the response to anti-CTLA-4 + anti-PD-1 in MC38 tumor-bearing mice (Figure 6C). Lastly, we examined the relevance of GC signaling in human cancer. We scored the single-cell data of TILs from melanoma patients pre- and post-ICB (Sade-Feldman et al., 2018) for expression of the GC signature. In line with our observations in B16F10 melanoma (Figure 1D), we found that the GC signature scored

highly in CD8$^+$ TILs that also scored highly for the T cell dysfunction signature (Figure 6D, **panels V** and **VI**). Most importantly, we found that expression of the GC signature in CD8$^+$ TILs positively correlated with non-responsiveness to ICB in both pre- ($p<2.2\times10^{-16}$) and post- ($p=3.246\times10^{-13}$) treatment samples (Figure 6D, **panel VII**). Altogether, these data indicated that GC signaling dampened anti-tumor immunity and ICB efficacy.

Glucocorticoid signaling can co-operate with other signaling pathways to amplify immunosuppression in the TME

The transactivation of multiple checkpoint receptors and IL-10 by the GR (Figure 4) were reminiscent of observations from our lab and others that IL-27 regulates a gene module that includes checkpoint receptors (Tim-3, Lag3, Tigit) and IL-10 and suppresses the responses of CD8$^+$ TILs (Chihara et al., 2018; DeLong et al., 2019; Zhu et al., 2015). GCs have been shown to work in concert with TFs such as the STAT family (Petta et al., 2016) and STAT1 and STAT3 are downstream of IL-27. We therefore examined the relationship of the GC and IL-27 signaling pathways. Unsupervised principle component analysis (PCA) of the RNA profiles from cells treated with GC, IL-27, or both showed that GC and IL-27 each induced a distinct RNA profile with GC + IL-27 treatment inducing the largest transcriptional change relative to control (Figure 7A, B and S7A). Examination of differentially expressed (DE) genes across all three conditions relative to control showed some common as well as some distinct genes (Figures 7C and S7B). 3,417 out of 6,812 DE genes between GC + IL-27 compared to control genes showed non-additive regulation (Figure 7C and Table S2) and 1,022 out of 6,812 DE genes overlapped with the dysfunction signature (Table S3 and Figure S7C). To determine the functional consequences of the GC + IL-27 signaling pathways on T cell effector function *in vivo*, we crossed E8i-Cre$^+$*Nr3c1*$^{fl/fl}$ mice with WSX1$^{-/-}$ (*IL27ra*$^{-/-}$) mice to generate double knock-out (DKO) mice. We isolated CD8$^+$ T cells from WT, E8i-Cre$^+$*Nr3c1*$^{fl/fl}$, WSX-1$^{-/-}$, or DKO mice and transferred them along with WT CD4$^+$ T cells into Rag-1$^{-/-}$ mice followed by implantation of MC38-Ova^{dim} colon carcinoma. In line with our previous findings, absence of either GC (Figure 3A and S4A) or IL-27 signaling (Zhu et al., 2015) alone individually conferred tumor growth control; however, the absence of both pathways led to significantly greater tumor growth inhibition (Figure 7D). We further identified that TADCs were the main source of IL-27 (p28 and EBi3) in the TME (Figure 7E). Thus, GC can partner with signaling pathways like IL-27 in CD8$^+$ TILs to further dampen their anti-tumor immune responses.

Discussion

Here, we uncovered an immunoregulatory circuit wherein GC production by tumor-associated monocyte-macrophage lineage cells regulates effector differentiation and development of dysfunction in CD8$^+$ TILs. The GR transactivated multiple checkpoint receptors together with IL-10 and repeated T cell activation in the presence of GC induced many dysfunction-associated genes, thus uncovering a mechanism by which GC signaling suppresses immune responses. Importantly, the presence of active GC signaling associated with failure to respond to checkpoint blockade in both pre-clinical models and in melanoma patients (Sade-Feldman et al., 2018), underscoring the clinical relevance of our findings.

Our data showing that GC signaling affects both effector transition and the development of dysfunction in $CD8^+$ TILs, raises the issue of how the GR mediates these different effects. It is known that GR-driven regulatory networks are highly cell type context dependent. Further, the GR has also been shown to remodel chromatin (Jubb et al., 2017). Thus, GR-driven transcriptional regulation in a given cellular context may be mediated by at least two non-mutually exclusive mechanisms, chromatin remodeling and partnering with the specific repertoire of TFs present (Weikum et al., 2017). The level of GR expression in a given cell may further influence the extent to which these mechanisms operate. Indeed, we observed a gradient of increasing GR expression and signaling from naïve to dysfunctional $CD8^+$ TILs. It is therefore possible that increasing GR signaling may underlie the orchestration of the distinct transcriptional and epigenetic programs present in naïve, effector, and dysfunctional $CD8^+$ TILs (Pauken et al., 2016; Philip et al., 2017; Sen et al., 2016). Of note, dysfunctional T cells have been shown to have increased chromatin accessibility at regions containing GR motifs (Satpathy et al., 2019).

Our findings indicate that low levels of GR signaling during initial T cell activation restrain effector transition by maintaining TCF-1, which is known to regulate effector T cell differentiation (Danilo et al., 2018; Tiemessen et al., 2014). Our observed reduction in TCF-1 expression in E8i-Cre^+ *Nr3c1*$^{fl/fl}$ $CD8^+$ TILs is in line with the demonstration by Yu *et al.* that RNAi of *Nr3c1* reduces TCF-1 expression in $CD8^+$ T cells in the context of bacterial infection (Yu et al., 2017). Yu *et al.* additionally demonstrate a role for the GR in the generation of memory precursor cells, likely via regulation of TCF-1. We do not examine a role for the GR in generating memory, rather, we show that the GR has a role in promoting T cell dysfunction. In this regard, a recent study showed that TCF-1 plays a critical role in maintaining the precursors of dysfunctional T cells in the context of chronic viral infection (Chen et al., 2019). In tumors, TCF-1 is important for maintaining stem-like $CD8^+$ T cells that seed the $CD8^+$ T cell effector pool upon checkpoint blockade (Kurtulus et al., 2019; Siddiqui et al., 2019). Our study shows that the loss of GR potentiates the response to checkpoint blockade, indicating that the ability of the stem-like $CD8^+$ T cell pool to seed the effector compartment is not compromised in E8i-Cre^+ *Nr3c1*$^{fl/fl}$ mice. Our data are consistent with a model where the loss of GR and GC signaling fine tunes the expression level of TCF-1, thereby accelerating the differentiation of precursors into effector $CD8^+$ T cells that do not develop dysfunction and rather enhance response to checkpoint blockade.

Our study focuses on the effects of endogenous GC in the TME; however, exogenous GC is often administered to cancer patients. In glioblastoma patients, Dex is given to prevent cerebral edema. How this impacts the ability of these patients to respond to ICB is not known (Kelly and Gilbert, 2020). GCs are also used as first-line agents for managing immune-related adverse events (IRAEs) (Kumar et al., 2017) associated with ICB. Although initial studies indicated that administration of GCs does not negatively impact therapeutic outcome (Beck et al., 2006; Downey et al., 2007; Johnson et al., 2015; Weber et al., 2008), a recent study comparing patients receiving either low- or high-dose GC for the treatment of IRAEs showed that patients who received high-dose GC had both reduced survival and time to treatment failure (Faje et al., 2018). Similarly, another study has shown reduced overall survival (OS) in melanoma patients who received corticosteroids along with ICB (Tokunaga et al., 2019). Lastly, baseline steroid has also been associated with poor response to

PD-1/PD-L1 ICB (Arbour et al., 2018). These observations highlight the need to understand the effects of low- versus high-dose administration of exogenous GCs and how these relate to the effects of endogenous GCs. Notwithstanding these considerations, we observed that patients who fail to respond to ICB (Sade-Feldman et al., 2018) have higher expression of the GC signature. Our findings have implications not only for the application of GCs to treat IRAEs in patients receiving checkpoint blockade but also suggest the application of either GC synthesis or signaling inhibitors to improve anti-tumor immune responses either alone or in combination with other modalities.

Limitations of Study

Our study highlights monocyte-macrophage lineage cells as one of the major sources of GC in colon carcinomas. Whether this or other cell types are the predominant source of extra-adrenal steroid in other cancer types remains to be determined. Further, whether the effects of any of the checkpoint receptors that are induced by Dex are responsible for the observed suppressive effects of Dex requires further investigation. Lastly, our study addresses the effects of GC signaling in $CD8^+$ T cells; however, GC signaling could also modulate the responses of other immune cells in the TME.

STAR*METHODS

Detailed methods are provided in the online version of this paper and include the following:

- **RESOURCE AVAILABILITY**
  - **Lead Contact—**Requests for reagents should be directed to and will be fulfilled by the Lead Contact, Ana C. Anderson (acanderson@bwh.harvard.edu).
  - **Materials Availability—**This study does not generate any unique reagents.
  - **Data and Code Availability—**The RNA-Sequencing datasets generated during this study are available at Gene Expression Omnibus (GEO) Repository with accession code GSE153556.
- **EXPERIMENTAL MODEL AND SUBJECT DETAILS**
  - **Mice—**6–8 week old male or female C57BL/6, *Nr3c1*$^{fl/fl}$, Rag1$^{-/-}$, E8iCre, WSX1$^{-/-}$ and LysM-Cre transgenic mice were purchased from the Jackson Laboratory. *Nr3c1*$^{fl/fl}$ was crossed to E8iCre and/or E8iCre x WSX1$^{-/-}$. Cryopreserved sperm from males bearing a targeted *Cyp11a1* allele were obtained from EUCOMM and used to fertilize C57BL/6 oocytes. Heterozygote progeny were confirmed by PCR and bred to mice that express the FlpO recombinase (MMRC, UC Davis) to remove the neomycin resistance cassette followed by breeding with LysM-Cre. All mice were housed under SPF conditions. All experiments involving laboratory animals were performed under protocols approved by the Harvard Medical Area Standing Committee on Animals (Boston, MA).
  - **Collection of colorectal carcinoma patient specimens—**Primary colorectal carcinoma specimens were obtained under informed consent from untreated patients

undergoing surgical resection at the Brigham and Women's /Dana Farber Cancer Center and Massachusetts General Hospital (IRB protocol 03–189 and 02–240). Freshly resected CRC tumors and adjacent normal colon were recovered in Medium 199 (Thermo Fisher) supplemented with 2% heat-inactivated FCS (Sigma Aldrich) and stored briefly on ice.

- **Tumor cell lines used—**MC38-Ova^{dim} was generously provided by Mark Smyth. B16F10 was purchased from ATCC. MC38 was generously provided by Carla Rothlin. MC38-Ova^{dim}-GFP was generated in our lab as follows, HEK293T cells were transfected with pLenti PGK GFP Puro plasmid. The resulting Lenti virus was then used to infect Mc38Ova^{dim} cell line to generate a GFP expressing cell line. MC38-Ova^{dim} (0.5×10^6) or B16F10 (0.25×10^6) and MC38-Ova^{dim} -GFP (0.5×10^6) cells were implanted subcutaneously into the right flank of mice.

- **METHOD DETAILS:**

  - **Cell culture and treatment with glucocorticoid—**CD8$^+$ T cells from splenocytes and lymph nodes were isolated using CD8 microbeads (Miltenyi). Cells were further stained with antibodies against CD8, CD62L and CD44, and CD8$^+$CD62L^{hi}CD44$^-$ naive cells were sorted by BD FacsAria (BD Biosciences). Sorted cells were cultured for 9 days as described below in DMEM supplemented with 10% (vol/vol) FCS, 50 mM mercaptoethanol, 1 mM sodium pyruvate, nonessential amino acids, L-glutamine, and 100 U/ml penicillin and 100 g/ml streptomycin. Specifically, naive CD8$^+$ cells were stimulated with plate bound anti-CD3 (145–2C11, 1 μg/ml) and anti-CD28 (PV-1, 1μg/ml) in the presence of either 10 nM dexamethasone (Sigma), 100 nM Corticosterone (Fisher Scientific), 25 ng/ml IL-27 (R&D), or both dexamethasone and IL27 for 3 days. Cells were then rested in the presence of 5 ng/ml IL2 (Miltenyi) for 3 days followed by restimulation with plate bound anti-CD3 (145–2C11, 1 μg/ml) and anti-CD28 (PV-1, 1μg/ml) in the presence of either 10nM dexamethasone (Sigma), 100 nM Corticosterone (Fisher Scientific), 25 ng/ml IL-27 (R&D), or both dexamethasone and IL27 for an additional 3 days.

  - **Human CD8$^+$ T cell culture—**Peripheral blood was procured from healthy volunteers. Mononuclear cells were enriched by density gradient centrifugation on Ficoll-Paque PLUS (GE Healthcare) in SepMate-50 tubes (Stem Cell Technologies). CD8$^+$ T cells were isolated from PBMCs using CD8 microbeads (Miltenyi) according to manufacturer protocol. Cells were further stained with antibodies against CD8, CD62L, CCR7 and CD45RA. Naïve cells CD8$^+$CD62L^{hi}CCR7$^+$CD45RA$^+$ cells were sorted by BD FacsAria (BD Biosciences). Sorted CD8$^+$ T cells were cultured for 9 days in RPMI supplemented with 10% (vol/vol) autologous heat-inactivated serum, 1 mM sodium pyruvate, 1X nonessential amino acids, 2mM L-glutamine, 100 U/ml penicillin, and 100 g/ml streptomycin. Naïve CD8$^+$cells were stimulated with plate-bound anti-CD3 (Biolegend, clone UCHT1, 1 μg/ml) and anti-CD28 (Biolegend, clone CD28.2, 1μg/ml) in the presence of 10nM dexamethasone (Sigma) or vehicle control for 3 days. Cells were then rested in the presence of 100U/ml IL2 (R&D Systems) for 3 days. Next, the cells were restimulated with plate-bound anti-CD3 (1 μg/ml)and anti-CD28 (1μg/ml) in the presence of either 10nM dexamethasone (Sigma) or vehicle control for 3 days.

- **Tumor experiments—**Tumor size was measured in two dimensions by caliper and is expressed as the product of two perpendicular diameters. In some experiments, mice were treated with anti-PD-1 (RMP1–14) (100 mg per mouse) antibodies or control immunoglobulin (Rat IgG2a) i.p. on days 5, 8 and 11 post-tumor implantation. Mice were then monitored for tumor growth. In some experiments, mice were treated with dexamethasone (Sigma) (10 mg/kg) or anti-PD1 (RMP1–14) +anti-CTLA-4 (9H10) (8 mg/kg) or both on Day 7 post-tumor implantation. Antibodies were administered bi-weekly for a total of 5 treatments (n=9–10). Dexamethasone was administered for 10 consecutive days.

- **Isolation of TILs—**TILs were isolated by dissociating tumor tissue in the presence of collagenase D (2.5 mg/ml) for 20 minutes prior to centrifugation on a discontinuous Percoll gradient (GE Healthcare). Isolated cells were then used in various assays.

- **Flow cytometry—**Single cell suspensions were stained with antibodies against surface molecules. For murine samples, antibodies against CD4 (RM4–5), CD8 (53–6.7), CD107a (1D4B), PD-1 (RMP1–30) CD45 (30-F11), CD3 (145–2C11), CD19 (6D5), NK1.1 (V=PK136), Ly-6C (HK1.4), Ly-6G (1A8), CD11b (M1/70), CD11c (N418), CD24 (M1/69), I-A/I-E (M5/114.15.2), F4/80 (BM8) CD103 (2E7), CD45.1 (A20), CD45.2 (104) were purchased from BioLegend. Antibodies against LAG-3 (C9B7W), Gzmb (NGZB) and Tigit (GIGD7) were purchased from eBioscience. Anti-Tim-3 (5D12) antibody was generated in house. Antibody against GR (G5) was purchased from Santa Cruz. Antibody against Siglec-F (E50–2440) was purchased from BD Biosciences. For human samples, antibodies against CD3 (UCHT1), CD8a (RPA-T8), Tim-3 (F38–2E2), PD-1 (EH12.2H7) Lag-3 (11C3C65), CCR7 (G043H7), CD62L(DREG-56) and CD45RA(HI100) were purchased from Biolegend and antibody against TIGIT (MBSA43) was purchased from Thermo Fisher. Fixable viability dye eF506 (eBioscience) or Zombie UV dye (Biolegend) were used to exclude dead cells. For GR staining, eBioscience Foxp3/transcription factor staining buffer set was used as per manufacturer's protocol. For intra-cellular cytokine (ICC) staining of $CD8^+$ T cells in culture *in vitro*, cells were stimulated with phorbol-12-myristate 13-acetate (PMA) (50ng/ml, Sigma-Aldrich) and ionomycin (1μg/ml, Sigma-Aldrich) in the presence of Golgi Plug (BD Biosciences) and Golgi Stop (BD Biosciences) for four hours prior to cell surface and ICC staining. For intra-cytoplasmic cytokine staining of TILs, cells were stimulated *in vitro* with 5 μg/ml OVA257–264 peptide (Sigma-Aldrich) for 4 hrs in the presence of Golgi stop (BD Biosciences) and Golgi Plug (BD Biosciences) prior to cell surface and ICC staining. Importantly, antibody detecting CD107a (1D4B) was added to the cells during stimulation. Following fixation and permeabilization, staining with antibodies against the following was performed for murine samples: IL-2 (JES6–5H4), TNF-a (MP6-XT22), IFN-g (XMG-1.2) and Granzyme B (GB11) were purchased from Biolegend. Antigen specific T cells were determined by H- 2Kb/ OVA257–264 dextramer staining following the manufacturer's protocol (Immudex). Cell proliferation was studied using CellTrace violet (Thermo Fisher Scientific) following manufacturer's protocol. All data were collected on a BD LsrII (BD Biosciences) or Fortessa (BD Biosciences) and analyzed with FlowJo 10.4.2 software (TreeStar).

- **Adoptive transfers—**For adoptive transfer experiments, $CD4^+$ ($FOXP3^+$ and $FOXP3^-$) and $CD8^+$ T cells from either WT, WT (CD45.1), *Nr3c1*$^{fl/fl}$ E8iCre, $WSX1^{-/-}$ or *Nr3c1*$^{fl/fl}$ E8iCre$^+$$WSX1^{-/-}$ (dKO) mice were isolated by cell sorting using a BD FACSAria. A total of 1.5×10^6 cells at a ratio of 1: 0.5 (CD4/CD8) was mixed in PBS and injected i.v. into $Rag^{-/-}$ mice. Two days later, mice were implanted with MC38-Ova^{dim} colon carcinoma cells and followed for tumor growth.

- ***In vivo* and *in vitro* modulation of glucocorticoid—**MC38-Ova^{dim} was implanted in wild type C57BL/6 mice and either Metyrapone (50mg/kg; Fisher Scientific), Corticosterone (2.5mg/kg) or vehicle control PBS (Gibco) was administered intra-tumorally on Day 5,6,7 and 9 post-tumor implantation. In some experiments, MC38-Ova^{dim} tumor explants or sorted $lin^-CD45^+CD24^-$ cells were cultured in the presence or absence of Metyrapone (25 or 50 ng/ml) for 24hrs. Supernatants were harvested and corticosterone measured by ELISA (Arbor Assays).

- **Measurement of steroids in tissue extracts—**Organic phase extraction using acetonitrile and hexane (1:2) was employed to extract steroids from tissues followed by examination of corticosterone (Arbor Assays) and/or pregnenolone (Abnova) by ELISA.

- **Luciferase assays—**HEK293T cells were transfected with firefly luciferase reporter constructs for IL-10, PD1, Tim3, Lag3 or Tigit, together with Renilla luciferase reporter as internal control and plasmids expressing *Nr3c1* or empty control vector. Dex or vehicle control was added to the culture 24hrs after transfection. Cells were analyzed at 24hrs after the addition of Dex with the dual luciferase assay kit (Promega). Fragments containing the proximal IL10 promoter (−1.5 kb including the $HSS^-0.12$ site), and the $HSS^+2.98$ region followed by of the IL10 minimal promoter were cloned into pGL4.10 Luciferase reporter plasmid (Promega). Fragments containing the cis-regulatory elements for the Havcr2 (chr11: 46474049–46474628, mm10) *Pdcd1 (*TSS +15kb, *chr1:* 94034621–94036002, mm10), Tigit (proximal promoter, - 2.5kb) and Lag3 (chr6: 124901592–124902407, mm10) loci were cloned into pGL4.23 Luciferase reporter plasmid (Promega).

- **Quantitative PCR—**Total RNA was extracted using RNeasy columns (Qiagen) or PicoPure™ RNA Isolation Kit (Thermo Fischer). Reverse transcription of mRNA was performed in a thermal cycler (Bio-Rad) using iScript cDNA Synthesis Kit (Bio-Rad) or SuperScript™ VILO™ cDNA Synthesis Kit (Thermo Fischer). qPCR was performed in the Vii7 Real-Time PCR system (Applied Biosystems) using the primers for Taqman gene expression (Applied Biosystems). Data were normalized to the expression of Actb.

- **RNA-Seq—**1,000 cells were sorted into 5 μL of Buffer TCL (Qiagen) supplemented with 1% 2 mercaptoethanol. Plates were thawed on ice for one minute and spun down at 2,000 rpm for one minute. Immediately following, RNA lysate was purified using a 2.2x RNAClean SPRI bead ratio (Beckman Coulter Genomics). The RNA captured beads were processed using a modified SMART-Seq2 protocol(Picelli et al., 2013) entailing RNA secondary structure denaturation (72˚C for three minutes), reverse transcription with Maxima Reverse Transcriptase (Life Technologies), and whole-transcription amplification (WTA) with KAPA HiFi HotStart ReadyMix 2X (Kapa Biosystems) for 11 cycles. WTA

products were purified with Ampure XP beads (Beckman Coulter), quantified with a Qubit dsDNA HS Assay Kit (ThermoFisher), and quality accessed with a high-sensitivity DNA chip (Agilent). 0.2 ng of purified WTA product was used as input for the Nextera XT DNA Library Preparation Kit (Illumina). Uniquely barcoded libraries were pooled and sequenced with a NextSeq 500 high output V2 75 cycle kit (Illumina) using 38 and 38 paired end reads(Picelli et al., 2013).

Computational analyses

Signature scoring in single cells: $CD8^+$ TILs single-cell data were obtained and processed as previously described(Singer et al., 2016). Briefly, Briefly, paired reads were mapped to mouse annotation mm10 using Bowtie (Langmead et al., 2009) (allowing a maximum of one mismatch in seed alignment, and suppressing reads that had more than 10 valid alignments) and TPMs were computed using RSEM(Li and Dewey, 2011), and log2(TPM+1) values were used for subsequent analyses. Next, we filtered out low quality cells and cell doublets, maintaining for subsequent analysis the 588 cells that had (1) 1,000–4,000 detected genes (defined by at least one mapped read), (2) at least 200,000 reads mapped to the transcriptome, and at least 50% of the reads mapped to the transcriptome. Here, we restricted the genes considered in subsequent analyses to be the 7,790 genes expressed at log2(TPM+1) R 2 in at least ten percent of the cells. After removal of low-quality cells/ genes, the data were normalized using quantile normalization followed by PCA. PCs 1–8 were chosen for subsequent analysis due to a drop in the proportion of variance explained following PC8. We used to visualize single cells in a two-dimensional non-linear embedding. To score each cell for a gene signature, expression data was initially scaled by calculating the z-score across each gene. For each gene signature, a cell-specific signature score was computed by first sorting the normalized scaled gene expression values for each cell followed by summing up the indices (ranks) of the signature genes. For signatures consisting of an induced and suppressed set of genes, two ranking scores were obtained separately, and the suppressed associated signature score was subtracted from the induced generated signature score. A contour plot was added on top of the tSNE space, which takes into account only those cells that have a signature score above the indicated threshold to further emphasize the region of highly scored cells.

RNA-Seq data pre-processing: RNA-seq reads were aligned using Tophat (Trapnell et al., 2009) (to mouse genome version mm9), and expression levels were calculated using RSEM(Li and Dewey, 2011) using annotated transcripts (mm9), followed by further processing using the Bioconductor package DESeq in R(Anders and Huber, 2010). The data was normalized using TMM normalization, and differentially expressed genes were defined using the differential expression pipeline on the raw counts with a single call to the function DESeq (FDR- adjusted p-value <0.05). Heatmap figures were generated using pheatmap package(Kolde and Vilo, 2015) and clustered using Euclidean distance.

Analysis of additive and non-additive effects: To test whether the glucocorticoid and IL-27 signaling pathways had additive or non-additive effects on gene expression, we stimulated naïve $CD8^+$ T cells in the presence of Dex, IL-27, or Dex+IL-27 *in vitro*. We tested for non-additive effects between IL-27 and glucocorticoid signaling using a negative

binomial generalized linear model in order to account for both estimations of the mean and the dispersion across conditions, where dispersion describes the relationship between the mean and variance. The model was applied to the expression data using ANOVA between a model that takes into account the interaction between IL27 and Dex versus no interaction. We found that 1,675 out of 3,496 differentially expressed genes (adjusted $P < 0.05$, likelihood ratio test and false discovery rate (FDR) correction) between control and Dex +IL-27 stimulated CD8+ cells have non-additive effects.

Analysis of human TILs data: Data was downloaded from(Sade-Feldman et al., 2018) in a in log2(TPM+1) format. PCA was performed after removal of non-expressed genes. PCs 1–8 were chosen for subsequent analysis due to a drop in the proportion of variance explained following PC8. We used tSNE(Maaten, 2008) to visualize single cells in a two-dimensional non-linear embedding. The glucocorticoid signature was projected onto single cell RNA profiles of TILs from 48 melanoma patients treated with checkpoint blockade (with 35 anti-PD-1, 11 anti-CTLA4+PD-1, and 2 anti-CTLA4 samples)(Sade-Feldman et al., 2018).

- **QUANTIFICATION AND STATISTICAL ANALYSIS**

Significant differences between two groups were analyzed using GraphPad Prism 8 using paired or unpaired two-tailed Student's t test or in case of multiple groups one-way or two-way ANOVA with multiple testing (Tukey). Tumor growth curves were analyzed using linear mixed effects models to test the trajectory of growth between various genotypes or treatments over time controlling for mouse. Differentially expressed genes following RNA-seq were defined using the differential expression pipeline on the raw counts with a single call to the function DESeq (FDR- adjusted p-value <0.05). Values of $*p < 0.05$, $**p < 0.01$, $***p < 0.001$ and **** $p<0.0001$ were considered statistically significant.

Supplementary Material

Refer to Web version on PubMed Central for supplementary material.

Acknowledgments

We thank Deneen Kozoriz for cell sorting. Dr. Sally Kent for advice on human T cell culture. Leslie Gaffney and Dr. Amit Bansal for figure preparation. This work was supported by grants from the National Institutes of Health (R01NS045937 to VKK, P01AI073748 to VKK and ACA, R01CA229400 to ACA) and by the Klarman Cell Observatory at the Broad Institute and HHMI. A.C.A. is a recipient of the Brigham and Women's President's Scholar Award. A.R. is an Investigator of the Howard Hughes Medical Institute. D.M is supported by SNSF postdoc mobility (P400PB_183910). G.E. is supported by EMBO Long Term Fellowship (ALTF 182–2018)

References

Abbaszade IG, Clarke TR, Park CH, and Payne AH (1995). The mouse 3 beta-hydroxysteroid dehydrogenase multigene family includes two functionally distinct groups of proteins. Mol Endocrinol 9, 1214–1222. [PubMed: 7491113]

Anders S, and Huber W. (2010). Differential expression analysis for sequence count data. Genome biology 11, R106.

Arbour KC, Mezquita L, Long N, Rizvi H, Auclin E, Ni A, Martinez-Bernal G, Ferrara R, Lai WV, Hendriks LEL, et al. (2018). Impact of Baseline Steroids on Efficacy of Programmed Cell Death-1 and Programmed Death-Ligand 1 Blockade in Patients With Non-Small-Cell Lung Cancer. J Clin Oncol 36, 2872–2878. [PubMed: 30125216]

Arriza JL, Weinberger C, Cerelli G, Glaser TM, Handelin BL, Housman DE, and Evans RM (1987). Cloning of human mineralocorticoid receptor complementary DNA: structural and functional kinship with the glucocorticoid receptor. Science 237, 268–275. [PubMed: 3037703]

Auphan N, DiDonato JA, Rosette C, Helmberg A, and Karin M. (1995). Immunosuppression by glucocorticoids: inhibition of NF-kappa B activity through induction of I kappa B synthesis. Science 270, 286–290. [PubMed: 7569976]

Bain PA, Yoo M, Clarke T, Hammond SH, and Payne AH (1991). Multiple forms of mouse 3 beta-hydroxysteroid dehydrogenase/delta 5-delta 4 isomerase and differential expression in gonads, adrenal glands, liver, and kidneys of both sexes. Proc Natl Acad Sci U S A 88, 8870–8874. [PubMed: 1924345]

Barrat FJ, Cua DJ, Boonstra A, Richards DF, Crain C, Savelkoul HF, de Waal-Malefyt R, Coffman RL, Hawrylowicz CM, and O'Garra A. (2002). In vitro generation of interleukin 10-producing regulatory CD4(+) T cells is induced by immunosuppressive drugs and inhibited by T helper type 1 (Th1)- and Th2-inducing cytokines. J Exp Med 195, 603–616. [PubMed: 11877483]

Beck KE, Blansfield JA, Tran KQ, Feldman AL, Hughes MS, Royal RE, Kammula US, Topalian SL, Sherry RM, Kleiner D, et al. (2006). Enterocolitis in patients with cancer after antibody blockade of cytotoxic T-lymphocyte-associated antigen 4. J Clin Oncol 24, 2283–2289. [PubMed: 16710025]

Bianchi M, Meng C, and Ivashkiv LB (2000). Inhibition of IL-2-induced Jak-STAT signaling by glucocorticoids. Proc Natl Acad Sci U S A 97, 9573–9578. [PubMed: 10920190]

Brattsand R, and Linden M. (1996). Cytokine modulation by glucocorticoids: mechanisms and actions in cellular studies. Aliment Pharmacol Ther 10 Suppl 2, 81–90; discussion 91–82. [PubMed: 8899106]

Cain DW, and Cidlowski JA (2017). Immune regulation by glucocorticoids. Nat Rev Immunol 17, 233–247. [PubMed: 28192415]

Carey KT, Tan KH, Ng J, Liddicoat DR, Godfrey DI, and Cole TJ (2013). Nfil3 is a glucocorticoid-regulated gene required for glucocorticoid-induced apoptosis in male murine T cells. Endocrinology 154, 1540–1552. [PubMed: 23425966]

Chen X, Oppenheim JJ, Winkler-Pickett RT, Ortaldo JR, and Howard OM (2006). Glucocorticoid amplifies IL-2-dependent expansion of functional FoxP3(+)CD4(+)CD25(+) T regulatory cells in vivo and enhances their capacity to suppress EAE. Eur J Immunol 36, 2139–2149. [PubMed: 16841298]

Chen Z, Ji Z, Ngiow SF, Manne S, Cai Z, Huang AC, Johnson J, Staupe RP, Bengsch B, Xu C, et al. (2019). TCF-1-Centered Transcriptional Network Drives an Effector versus Exhausted CD8 T Cell-Fate Decision. Immunity 51, 840–855 e845. [PubMed: 31606264]

Chihara N, Madi A, Kondo T, Zhang H, Acharya N, Singer M, Nyman J, Marjanovic ND, Kowalczyk MS, Wang C, et al. (2018). Induction and transcriptional regulation of the co-inhibitory gene module in T cells. Nature 558, 454–459. [PubMed: 29899446]

Clarke TR, Bain PA, Greco TL, and Payne AH (1993). A novel mouse kidney 3 beta-hydroxysteroid dehydrogenase complementary DNA encodes a 3-ketosteroid reductase instead of a 3 beta-hydroxysteroid dehydrogenase/delta 5-delta 4-isomerase. Mol Endocrinol 7, 1569–1578. [PubMed: 8145763]

Danilo M, Chennupati V, Silva JG, Siegert S, and Held W. (2018). Suppression of Tcf1 by Inflammatory Cytokines Facilitates Effector CD8 T Cell Differentiation. Cell Rep 22, 2107–2117. [PubMed: 29466737]

DeLong JH, O'Hara Hall A, Rausch M, Moodley D, Perry J, Park J, Phan AT, Beiting DP, Kedl RM, Hill JA, and Hunter CA (2019). IL-27 and TCR Stimulation Promote T Cell Expression of Multiple Inhibitory Receptors. Immunohorizons 3, 13–25. [PubMed: 31356173]

Downey SG, Klapper JA, Smith FO, Yang JC, Sherry RM, Royal RE, Kammula US, Hughes MS, Allen TE, Levy CL, et al. (2007). Prognostic factors related to clinical response in patients with metastatic melanoma treated by CTL-associated antigen-4 blockade. Clin Cancer Res 13, 6681–6688. [PubMed: 17982122]

Faje AT, Lawrence D, Flaherty K, Freedman C, Fadden R, Rubin K, Cohen J, and Sullivan RJ (2018). High-dose glucocorticoids for the treatment of ipilimumab-induced hypophysitis is associated with reduced survival in patients with melanoma. Cancer 124, 3706–3714. [PubMed: 29975414]

Fourcade J, Sun Z, Benallaoua M, Guillaume P, Luescher IF, Sander C, Kirkwood JM, Kuchroo V, and Zarour HM (2010). Upregulation of Tim-3 and PD-1 expression is associated with tumor antigen-specific CD8+ T cell dysfunction in melanoma patients. J Exp Med 207, 2175–2186. [PubMed: 20819923]

Hu Y, Tian W, Zhang LL, Liu H, Yin GP, He BS, and Mao XM (2012). Function of regulatory T-cells improved by dexamethasone in Graves' disease. Eur J Endocrinol 166, 641–646. [PubMed: 22219499]

Jin HT, Anderson AC, Tan WG, West EE, Ha SJ, Araki K, Freeman GJ, Kuchroo VK, and Ahmed R. (2010). Cooperation of Tim-3 and PD-1 in CD8 T-cell exhaustion during chronic viral infection. Proc Natl Acad Sci U S A 107, 14733–14738. [PubMed: 20679213]

Johnson DB, Friedman DL, Berry E, Decker I, Ye F, Zhao S, Morgans AK, Puzanov I, Sosman JA, and Lovly CM (2015). Survivorship in Immune Therapy: Assessing Chronic Immune Toxicities, Health Outcomes, and Functional Status among Long-term Ipilimumab Survivors at a Single Referral Center. Cancer Immunol Res 3, 464–469. [PubMed: 25649350]

Jonat C, Rahmsdorf HJ, Park KK, Cato AC, Gebel S, Ponta H, and Herrlich P. (1990). Antitumor promotion and antiinflammation: down-modulation of AP-1 (Fos/Jun) activity by glucocorticoid hormone. Cell 62, 1189–1204. [PubMed: 2169351]

Jubb AW, Boyle S, Hume DA, and Bickmore WA (2017). Glucocorticoid Receptor Binding Induces Rapid and Prolonged Large-Scale Chromatin Decompaction at Multiple Target Loci. Cell Rep 21, 3022–3031. [PubMed: 29241532]

Karin M, and Herschman HR (1979). Dexamethasone stimulation of metallothionein synthesis in HeLa cell cultures. Science 204, 176–177. [PubMed: 432639]

Karwacz K, Miraldi ER, Pokrovskii M, Madi A, Yosef N, Wortman I, Chen X, Watters A, Carriero N, Awasthi A, et al. (2017). Critical role of IRF1 and BATF in forming chromatin landscape during type 1 regulatory cell differentiation. Nat Immunol 18, 412–421. [PubMed: 28166218]

Kelly WJ, and Gilbert MR (2020). Glucocorticoids and immune checkpoint inhibitors in glioblastoma. J Neurooncol.

Kolde R, and Vilo J. (2015). GOsummaries: an R Package for Visual Functional Annotation of Experimental Data. F1000Research 4, 574. [PubMed: 26913188]

Kumar V, Chaudhary N, Garg M, Floudas CS, Soni P, and Chandra AB (2017). Current Diagnosis and Management of Immune Related Adverse Events (irAEs) Induced by Immune Checkpoint Inhibitor Therapy. Front Pharmacol 8, 49. [PubMed: 28228726]

Kurtulus S, Madi A, Escobar G, Klapholz M, Nyman J, Christian E, Pawlak M, Dionne D, Xia J, Rozenblatt-Rosen O, et al. (2019). Checkpoint Blockade Immunotherapy Induces Dynamic Changes in PD-1(−)CD8(+) Tumor-Infiltrating T Cells. Immunity 50, 181–194 e186. [PubMed: 30635236]

Langmead B, Trapnell C, Pop M, and Salzberg SL (2009). Ultrafast and memoryefficient alignment of short DNA sequences to the human genome. Genome Biol 10, R25.

Li B, and Dewey CN (2011). RSEM: accurate transcript quantification from RNA-Seq data with or without a reference genome. BMC Bioinformatics 12, 323. [PubMed: 21816040]

Ling Y, Cao X, Yu Z, and Ruan C. (2007). Circulating dendritic cells subsets and CD4+Foxp3+ regulatory T cells in adult patients with chronic ITP before and after treatment with high-dose dexamethasome. Eur J Haematol 79, 310–316. [PubMed: 17692100]

Maaten L.v.d., and Hinton G. (2008). Visualizing Data using t-SNE. J Machine Learning Research 9,, 2579–2605.

Munck A, Guyre PM, and Holbrook NJ (1984). Physiological functions of glucocorticoids in stress and their relation to pharmacological actions. Endocr Rev 5, 25–44. [PubMed: 6368214]

Oakley RH, and Cidlowski JA (2013). The biology of the glucocorticoid receptor: new signaling mechanisms in health and disease. J Allergy Clin Immunol 132, 1033–1044. [PubMed: 24084075]

Oh KS, Patel H, Gottschalk RA, Lee WS, Baek S, Fraser IDC, Hager GL, and Sung MH (2017). Anti-Inflammatory Chromatinscape Suggests Alternative Mechanisms of Glucocorticoid Receptor Action. Immunity 47, 298–309 e295. [PubMed: 28801231]

Pauken KE, Sammons MA, Odorizzi PM, Manne S, Godec J, Khan O, Drake AM, Chen Z, Sen DR, Kurachi M, et al. (2016). Epigenetic stability of exhausted T cells limits durability of reinvigoration by PD-1 blockade. Science 354, 1160–1165. [PubMed: 27789795]

Payne AH, and Hales DB (2004). Overview of steroidogenic enzymes in the pathway from cholesterol to active steroid hormones. Endocr Rev 25, 947–970. [PubMed: 15583024]

Petta I, Dejager L, Ballegeer M, Lievens S, Tavernier J, De Bosscher K, and Libert C. (2016). The Interactome of the Glucocorticoid Receptor and Its Influence on the Actions of Glucocorticoids in Combatting Inflammatory and Infectious Diseases. Microbiol Mol Biol Rev 80, 495–522. [PubMed: 27169854]

Philip M, Fairchild L, Sun L, Horste EL, Camara S, Shakiba M, Scott AC, Viale A, Lauer P, Merghoub T, et al. (2017). Chromatin states define tumour-specific T cell dysfunction and reprogramming. Nature 545, 452–456. [PubMed: 28514453]

Phuc Le P, Friedman JR, Schug J, Brestelli JE, Parker JB, Bochkis IM, and Kaestner KH (2005). Glucocorticoid receptor-dependent gene regulatory networks. PLoS Genet 1, e16.

Picelli S, Bjorklund AK, Faridani OR, Sagasser S, Winberg G, and Sandberg R. (2013). Smart-seq2 for sensitive full-length transcriptome profiling in single cells. Nat Methods 10, 1096–1098. [PubMed: 24056875]

Piemonti L, Monti P, Allavena P, Sironi M, Soldini L, Leone BE, Socci C, and Di Carlo V. (1999). Glucocorticoids affect human dendritic cell differentiation and maturation. J Immunol 162, 6473–6481. [PubMed: 10352262]

Quatrini L, Wieduwild E, Escaliere B, Filtjens J, Chasson L, Laprie C, Vivier E, and Ugolini S. (2018). Endogenous glucocorticoids control host resistance to viral infection through the tissue-specific regulation of PD-1 expression on NK cells. Nat Immunol 19, 954–962. [PubMed: 30127438]

Rhen T, and Cidlowski JA (2005). Antiinflammatory action of glucocorticoids--new mechanisms for old drugs. N Engl J Med 353, 1711–1723. [PubMed: 16236742]

Sade-Feldman M, Yizhak K, Bjorgaard SL, Ray JP, de Boer CG, Jenkins RW, Lieb DJ, Chen JH, Frederick DT, Barzily-Rokni M, et al. (2018). Defining T Cell States Associated with Response to Checkpoint Immunotherapy in Melanoma. Cell 175, 998–1013 e1020. [PubMed: 30388456]

Sakuishi K, Apetoh L, Sullivan JM, Blazar BR, Kuchroo VK, and Anderson AC (2010). Targeting Tim-3 and PD-1 pathways to reverse T cell exhaustion and restore antitumor immunity. J Exp Med 207, 2187–2194. [PubMed: 20819927]

Satpathy AT, Granja JM, Yost KE, Qi Y, Meschi F, McDermott GP, Olsen BN, Mumbach MR, Pierce SE, Corces MR, et al. (2019). Massively parallel single-cell chromatin landscapes of human immune cell development and intratumoral T cell exhaustion. Nat Biotechnol 37, 925–936. [PubMed: 31375813]

Scheinman RI, Cogswell PC, Lofquist AK, and Baldwin AS Jr. (1995). Role of transcriptional activation of I kappa B alpha in mediation of immunosuppression by glucocorticoids. Science 270, 283–286. [PubMed: 7569975]

Sen DR, Kaminski J, Barnitz RA, Kurachi M, Gerdemann U, Yates KB, Tsao HW, Godec J, LaFleur MW, Brown FD, et al. (2016). The epigenetic landscape of T cell exhaustion. Science 354, 1165–1169. [PubMed: 27789799]

Siddiqui I, Schaeuble K, Chennupati V, Fuertes Marraco SA, Calderon-Copete S, Pais Ferreira D, Carmona SJ, Scarpellino L, Gfeller D, Pradervand S, et al. (2019). Intratumoral Tcf1(+)PD-1(+)CD8(+) T Cells with Stem-like Properties Promote Tumor Control in Response to Vaccination and Checkpoint Blockade Immunotherapy. Immunity 50, 195–211 e110. [PubMed: 30635237]

Sidler D, Renzulli P, Schnoz C, Berger B, Schneider-Jakob S, Fluck C, Inderbitzin D, Corazza N, Candinas D, and Brunner T. (2011). Colon cancer cells produce immunoregulatory glucocorticoids. Oncogene 30, 2411–2419. [PubMed: 21258413]

Singer M, Wang C, Cong L, Marjanovic ND, Kowalczyk MS, Zhang H, Nyman J, Sakuishi K, Kurtulus S, Gennert D, et al. (2016). A Distinct Gene Module for Dysfunction Uncoupled from Activation in Tumor-Infiltrating T Cells. Cell 166, 1500–1511 e1509. [PubMed: 27610572]

Smoak KA, and Cidlowski JA (2004). Mechanisms of glucocorticoid receptor signaling during inflammation. Mech Ageing Dev 125, 697–706. [PubMed: 15541765]

Suarez A, Lopez P, Gomez J, and Gutierrez C. (2006). Enrichment of CD4+ CD25high T cell population in patients with systemic lupus erythematosus treated with glucocorticoids. Ann Rheum Dis 65, 1512–1517. [PubMed: 16606650]

Tiemessen MM, Baert MR, Kok L, van Eggermond MC, van den Elsen PJ, Arens R, and Staal FJ (2014). T Cell factor 1 represses CD8+ effector T cell formation and function. J Immunol 193, 5480–5487. [PubMed: 25355919]

Tokunaga A, Sugiyama D, Maeda Y, Warner AB, Panageas KS, Ito S, Togashi Y, Sakai C, Wolchok JD, and Nishikawa H. (2019). Selective inhibition of low-affinity memory CD8(+) T cells by corticosteroids. J Exp Med.

Trapnell C, Pachter L, and Salzberg SL (2009). TopHat: discovering splice junctions with RNA-Seq. Bioinformatics 25, 1105–1111. [PubMed: 19289445]

Weber JS, O'Day S, Urba W, Powderly J, Nichol G, Yellin M, Snively J, and Hersh E. (2008). Phase I/II study of ipilimumab for patients with metastatic melanoma. J Clin Oncol 26, 5950–5956. [PubMed: 19018089]

Weikum ER, Knuesel MT, Ortlund EA, and Yamamoto KR (2017). Glucocorticoid receptor control of transcription: precision and plasticity via allostery. Nat Rev Mol Cell Biol 18, 159–174. [PubMed: 28053348]

Wherry EJ, and Kurachi M. (2015). Molecular and cellular insights into T cell exhaustion. Nat Rev Immunol 15, 486–499. [PubMed: 26205583]

Xing K, Gu B, Zhang P, and Wu X. (2015). Dexamethasone enhances programmed cell death 1 (PD-1) expression during T cell activation: an insight into the optimum application of glucocorticoids in anti-cancer therapy. BMC Immunol 16, 39. [PubMed: 26112261]

Yang H, Xia L, Chen J, Zhang S, Martin V, Li Q, Lin S, Chen J, Calmette J, Lu M, et al. (2019). Stress-glucocorticoid-TSC22D3 axis compromises therapy-induced antitumor immunity. Nat Med 25, 1428–1441. [PubMed: 31501614]

Yang-Yen HF, Chambard JC, Sun YL, Smeal T, Schmidt TJ, Drouin J, and Karin M. (1990). Transcriptional interference between c-Jun and the glucocorticoid receptor: mutual inhibition of DNA binding due to direct protein-protein interaction. Cell 62, 1205–1215. [PubMed: 2169352]

Yu B, Zhang K, Milner JJ, Toma C, Chen R, Scott-Browne JP, Pereira RM, Crotty S, Chang JT, Pipkin ME, et al. (2017). Epigenetic landscapes reveal transcription factors that regulate CD8+ T cell differentiation. Nat Immunol 18, 573–582. [PubMed: 28288100]

Zhu C, Sakuishi K, Xiao S, Sun Z, Zaghouani S, Gu G, Wang C, Tan DJ, Wu C, Rangachari M, et al. (2015). An IL-27/NFIL3 signalling axis drives Tim-3 and IL-10 expression and T-cell dysfunction. Nature communications 6, 6072.

Highlights

- Endogenous glucocorticoid signaling shapes $CD8^+$ T cell differentiation in tumors
- The glucocorticoid receptor transactivates IL-10 and checkpoint receptor expression
- Tumor monocyte-macrophage lineage cells produce glucocorticoid which dampens antitumor immunity
- Glucocorticoid signaling in tumor microenvironment reduces immune checkpoint blockade efficacy

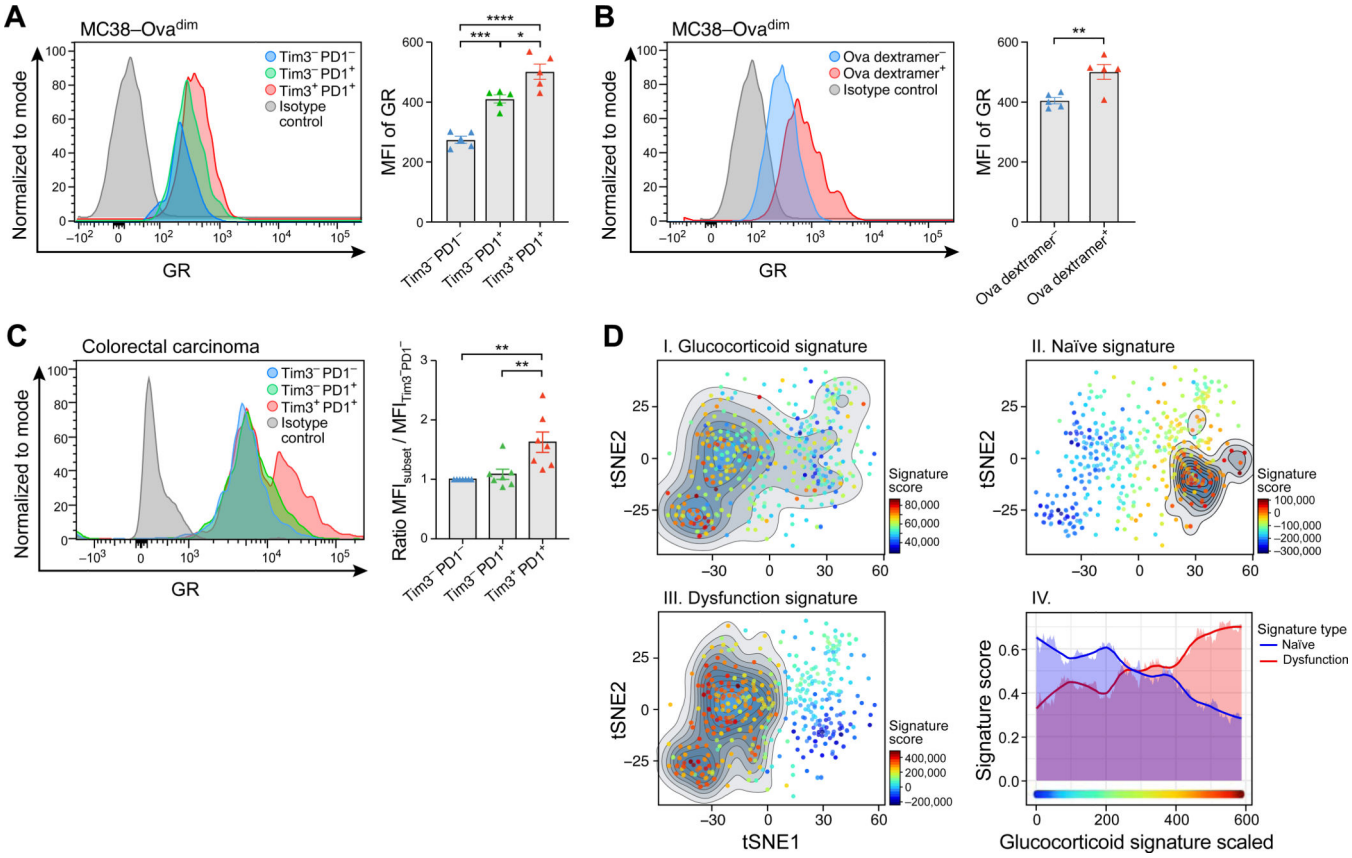

Figure 1: A gradient of glucocorticoid receptor expression and signaling in CD8$^+$ TILs

GR expression in TILs harvested from mice bearing MC38-Ova^{dim} colon carcinoma (tumor size 100–120 mm^2) (A,B) or from human colon carcinoma (C).

A) Representative histograms of GR expression and summary data of mean fluorescence intensity (MFI) in the indicated CD8$^+$ TILs populations. (n=5)

B) Representative histograms of GR expression and summary data of MFI in OVA-specific CD8$^+$ TILs. (n=5)

C) Representative histograms of GR expression and summary data of MFI in CD8$^+$ TILs. Data are normalized to the expression level in Tim-3$^-$PD-1$^-$ CD8$^+$ TILs. (n=7)

D) tSNE plot showing projection of a (I) GC signature, (II) naïve CD8$^+$T cell signature, (III) CD8$^+$ T cell dysfunction signature onto the single-cell RNA profiles of CD8$^+$ TILs (Singer et al., 2016). The contour marks cells showing highest expression and the color scale indicates low (blue) to high (red) expressing cells. (IV) Each cell in the dataset was scored for the three normalized signatures: GC, Naïve, and Dysfunction. Cells were then sorted based on their expression of the glucocorticoid signature from low (blue) to high (red) (x-Axis). The y-axis indicates the naive (blue) and dysfunction (red) signature score for each of the sorted cells. Moving average (shaded area) and smoothing conditional means (solid line) was used to aid visualization.

*p < 0.05, **p < 0.01, ***p < 0.001, ****p < 0.0001. One-way ANOVA (Tukey's multiple comparisons test) or unpaired Student's t test. Mean ± SEM is shown.

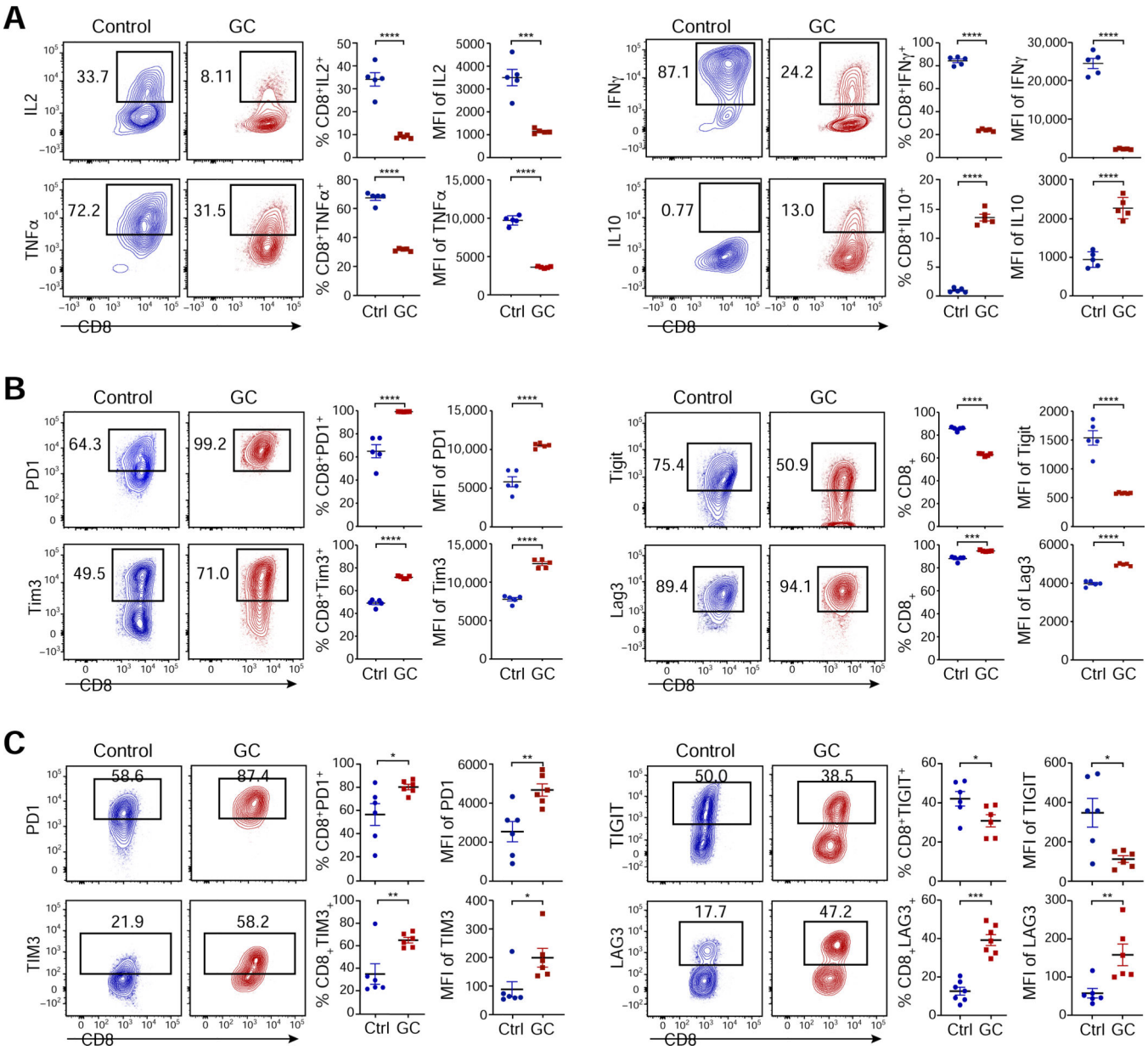

Figure 2: Glucocorticoid signaling promotes checkpoint receptor expression and dampens CD8$^+$ T cell effector functions

Murine (A-B) or human (C) naïve CD8$^+$ T cells were repeatedly activated (anti-CD3/28) in the presence or absence of GC (Dex). Data shown are representative of 3 independent experiments

B) Representative flow cytometry data and summary plots of the frequency and MFI the indicated cytokines following polyclonal activation (n=5)

B and C) Representative flow cytometry data and summary plots of the frequency and MFI of the indicated checkpoint receptors (n=5 for B), (n=6 for C)

*p<0.05, **p <0.01, ***p < 0.001, ****p<0.0001, unpaired Student's t test. Mean ± SEM is shown.

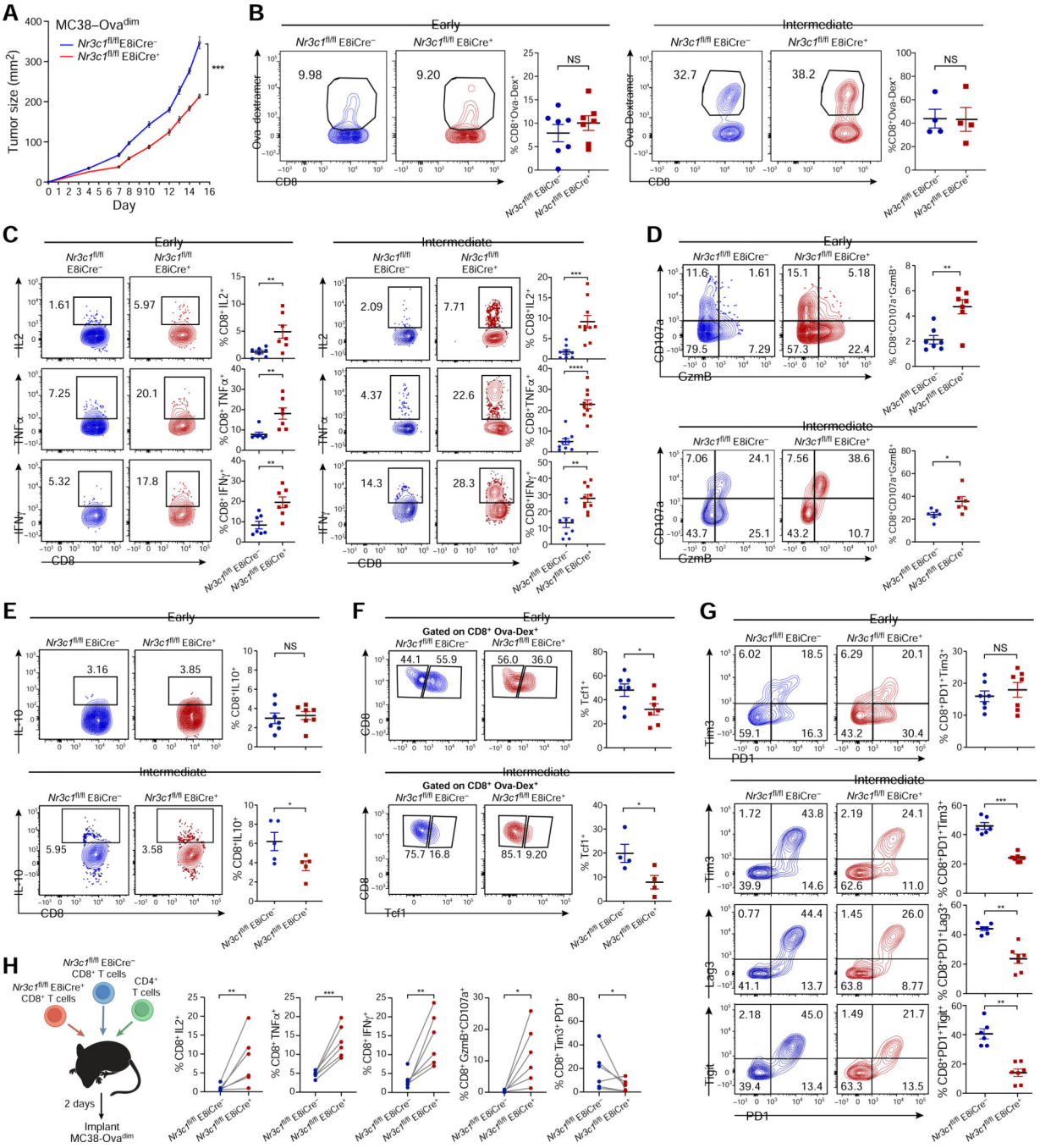

Figure 3: Glucocorticoid signaling regulates effector differentiation in CD8⁺ TILs

A) MC38-Ova^{dim} was implanted into WT (E8i-Cre^{-}*Nr3c1*$^{fl/fl}$) and E8i-Cre^{+}*Nr3c1*$^{fl/fl}$ mice (n=8–9). Mean tumor growth is shown, ***p< 0.001, linear mixed model. Data are representative of 3 independent experiments.

B-G) TILs were harvested from mice bearing MC38-Ova^{dim} at early (size 40–60 mm^2) and intermediate (size 120–150 mm^2) stages of tumor progression as determined by the growth observed in WT controls.

B) Representative flow cytometry data and summary plots of the frequency of OVA-specific $CD8^+$ TILs at early (n=7) and intermediate (n=4) stages.
(C-E) TILs were activated with $OVA_{257–264}$ followed by intracellular staining.
C) Representative flow cytometry data and summary plots of the frequency of the indicated cytokines in $CD8^+$ TILs at early (n=7) and intermediate (n=9–10) stages. Data are pooled from 2 independent experiments for the intermediate stage.
D) Representative flow cytometry data and summary plot of frequency of $CD107a^+$ $GzmB^+$ $CD8^+$ TILs at early (n=7) and intermediate (n=6) stages.
E) Representative flow cytometry data and summary plot of frequency of IL10-producing$CD8^+$ TILs at early (n=7) and intermediate (n=5) stages.
F) Representative flow cytometry data and summary plot of frequency of TCF-1^+ cells within Ova-specific $CD8^+$ TILs at early (n=7) and intermediate (n=4) stages.
G) Representative flow cytometry data and summary plot of frequency of checkpoint receptor expressing $CD8^+$ TILs at early (n=7) and intermediate (n=6–7) stages. NS, not significant, **p<0.01, ***p< 0.001, unpaired Student's t-test. Mean ± SEM are shown.
H) Experimental design: congenically marked WT (blue) and E8i-Cre^+*Nr3c1*$^{fl/fl}$ (red) $CD8^+$ T cells were transferred to $Rag^{-/-}$ recipients along with WT $CD4^+$ T cells (green). MC38-Ova^{dim} was implanted 2 days post T cell transfer. TILs were harvested at the intermediate stage of tumor growth and analyzed (n=6).
NS, not significant, *p< 0.05, **p<0.01, ***p<0.001, ****p<0.0001, unpaired Student's t-test or paired Student's t-test (H). Mean ± SEM are shown.

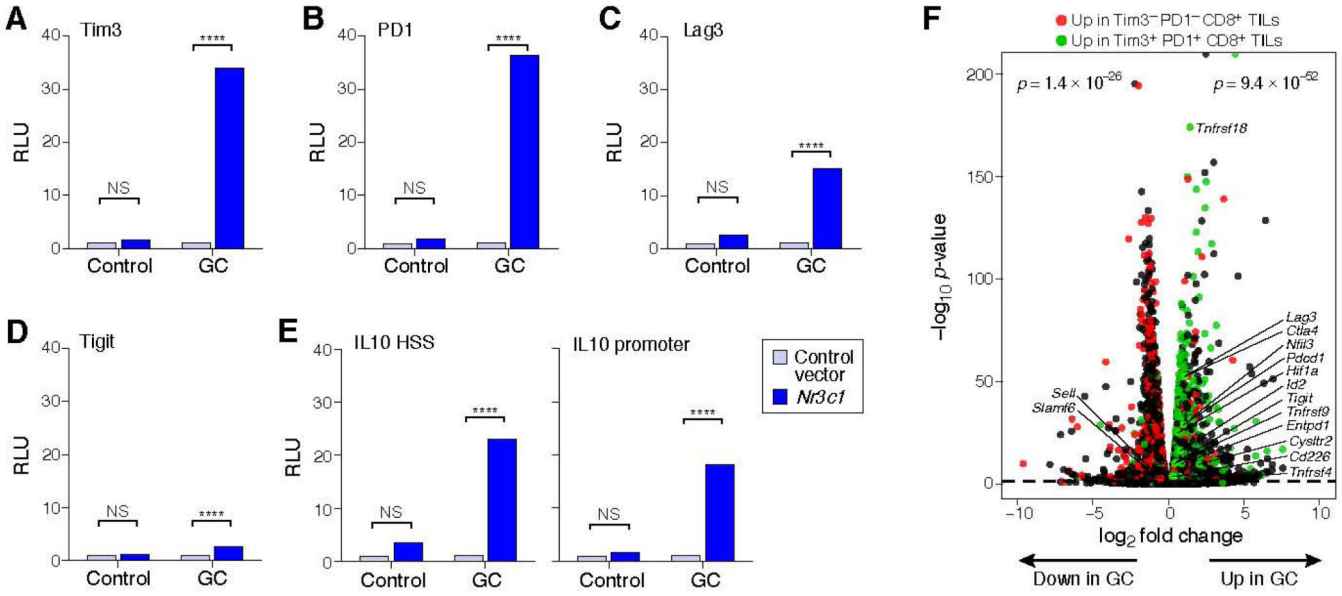

Figure 4: Glucocorticoid signaling transactivates checkpoint receptor and IL-10 expression and induces T cell dysfunction genes

(A-E) Luciferase activity in 293T cells transfected with pGL4.23 or pGL4.10 luciferase reporters for the loci of the indicated checkpoint receptors or IL10 together with either empty vector (control) or vector encoding *Nr3c1*. Cells were treated with GC (Dex) after 24h. Firefly luciferase activity was measured 48 h after transfection and is presented relative to constitutive Renilla luciferase activity. NS, not significant, ****p<0.0001, two-way ANOVA (Tukey's multiple comparisons test). Data are mean ± SEM and are representative of 2 independent experiments.

F) Volcano plot showing the overlap of genes suppressed by GC (Dex) with genes expressed in Tim-3^{-}PD-1^{-} CD8^{+} TILs ($p=1.4.0\times10^{-26}$) and genes induced by GC (Dex) with Tim-3^{+}PD-1^{+} CD8^{+} TILs ($p=9.4\times10^{-52}$) (Mean-rank Gene Set Test).

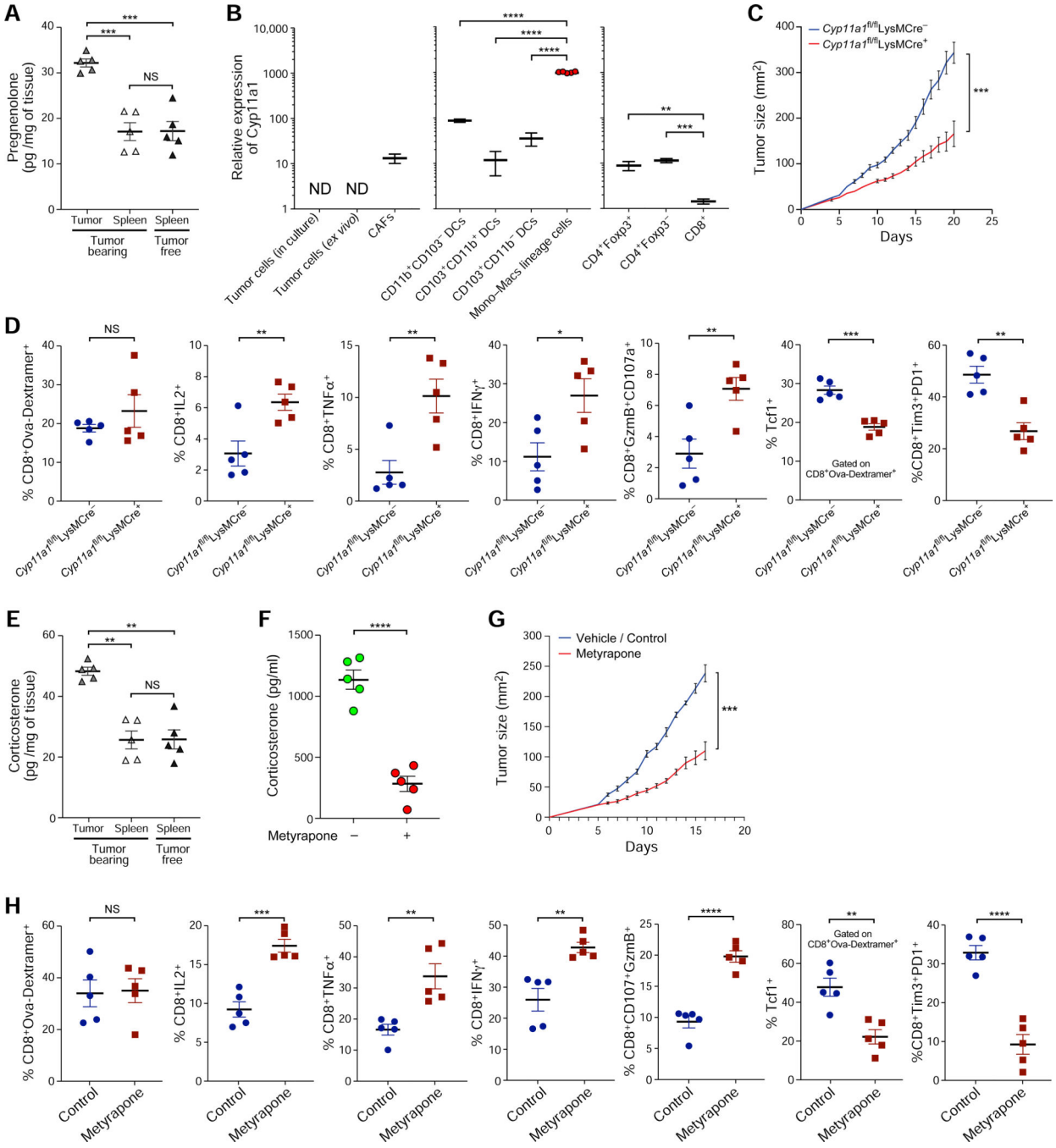

Figure 5: Intra-tumoral production of glucocorticoid affects tumor progression

A) Pregnenolone levels in the indicated tissues were quantified by ELISA (n=5).

B) qPCR analysis of *Cyp11a1* mRNA expression in the indicated cells. Data are pooled from 2 independent experiments (n= 5–6).

C) MC38-Ova^{dim} was implanted in LysMCre^{-} *Cyp11a1*$^{fl/fl}$ and LysMCre^{+}*Cyp11a1*$^{fl/fl}$ mice (n=5). Mean tumor growth is shown, ***p<0.001, linear mixed model. Data are representative of 2 independent experiments.

D) Analysis of $CD8^+$TILs at early stage of tumor development (tumor size 40–60 mm^2) (n=5)
E) Corticosterone levels were quantified by ELISA (n=5).
F) $Lin^-CD45^+CD24^-$ monocyte-macrophage lineage cells were isolated from MC38-Ova^{dim} tumors and cultured in the presence or absence of Metyrapone. At 24hrs corticosterone levels were quantified by ELISA (n=5).
G) MC38-Ova^{dim} was implanted in WT mice (n=5). Metyrapone or vehicle control was administered intra-tumorally on Days 5,6,7 and 9 post-tumor implantation. Mean tumor growth is shown ***p< 0.001, linear mixed model. Data are representative of 2 independent experiments.
H) MC38-Ova^{dim} was implanted in WT mice (n=5). Metyrapone or vehicle control was administered intra-tumorally on Days 5 and 6 post-tumor implantation. 24hrs later, TILs were harvested (tumor size 55–65 mm^2 in both groups) and analyzed by flow cytometry. Summary plots show the frequency of the indicated populations.
ND, not detected, NS, not significant *p<0.05 **p<0.01, ***p<0.001, ****p<0.0001, unpaired Student's t-test or One-way ANOVA (Tukey's multiple comparisons test). Data are mean ± SEM.

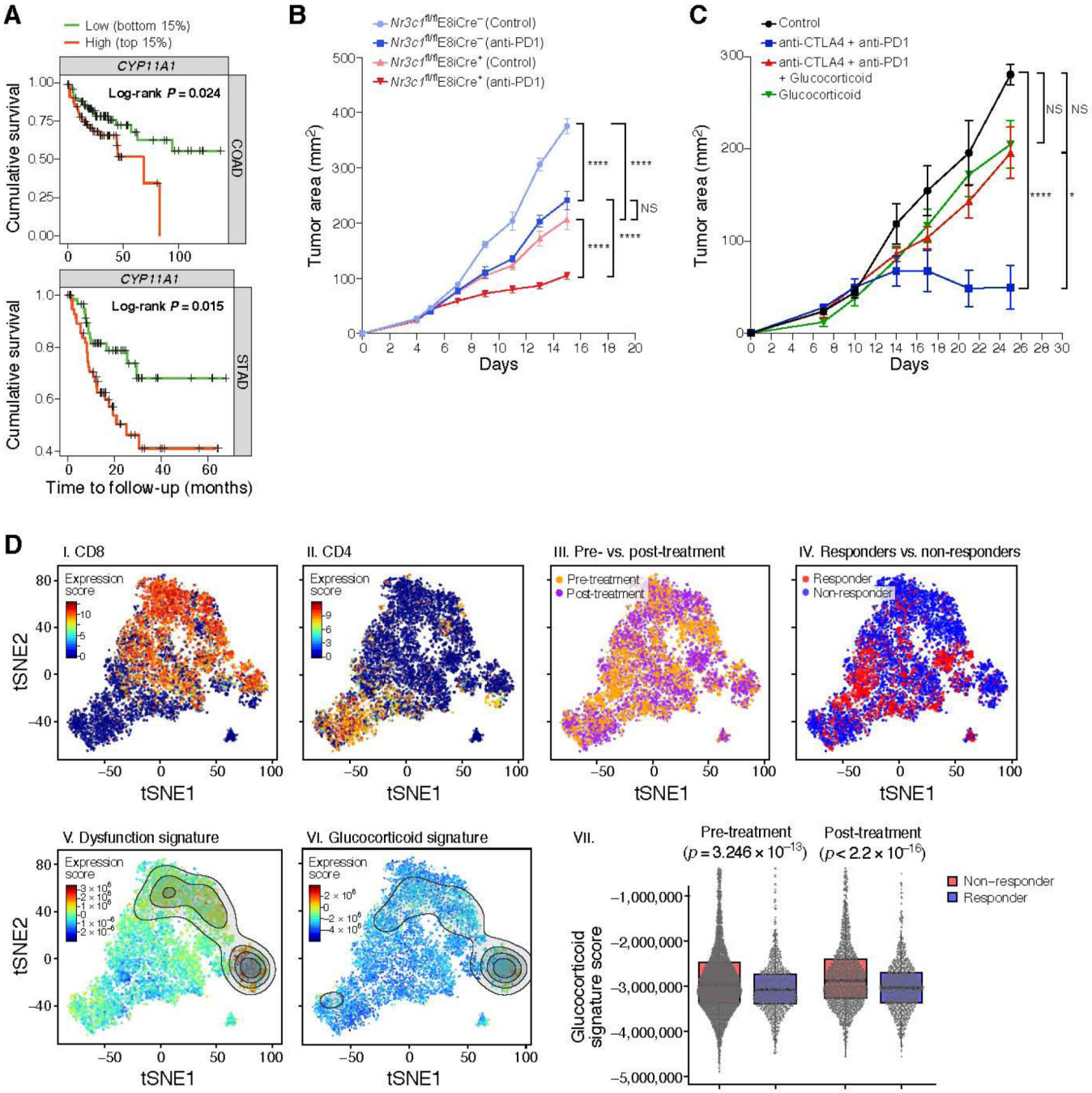

Figure 6: Glucocorticoid signaling in CD8$^+$ T cells affects responses to immunotherapy

A) Correlation of *Cyp11a1* mRNA expression with survival in patients with colon adenocarcinoma (COAD) and stomach adenocarcinoma (STAD) using TIMER.

B) MC38-Ova^{dim} was implanted into WT (E8i-Cre$^-$*Nr3c1*$^{fl/fl}$) and E8i-Cre$^+$*Nr3c1*$^{fl/fl}$ mice (n=7–8). Anti-PD1 was administered i.p on Days 5,8 and 11. Mean tumor growth is shown. NS, not significant, ****p< 0.0001, linear mixed model.

C) MC38 was implanted into WT mice. On Day 7 post-tumor implantation, mice were treated with GC (Dex) or anti-PD1+anti-CTLA-4 or both. Antibody was administered bi-

weekly for a total of 5 treatments (n=6–10). GC was administered for 10 consecutive days. NS, not significant, *p<0.05, ***p<0.001, linear mixed model.

D) tSNE plot of single-cell TILs data from melanoma patients treated with anti-PD-1, anti-CTLA-4, or anti-CTLA-4 + anti-PD-1(Sade-Feldman et al., 2018). I) CD8 expression, II) CD4 expression, III) pre- (orange) versus post- (purple) treatment samples, IV) Responder (red) versus non-responder (blue), V) Projection of $CD8^+$ TILs dysfunction signature, VI) Projection of the GC signature. VII) Box plots show the GC signature score in responder versus non-responders in pre- ($p=3.246\times10^{-13}$) and post- ($p <2.2\times10^{-16)}$ treatment samples (Welch Two Sample t-test). The lower and upper hinges correspond to the first and third quartiles. The upper and lower whiskers extend from the hinge to the largest and smallest value no further than 1.5 times the distance between the first and third quartiles, respectively. Data beyond the end of the whiskers are outlying points and are not plotted individually.

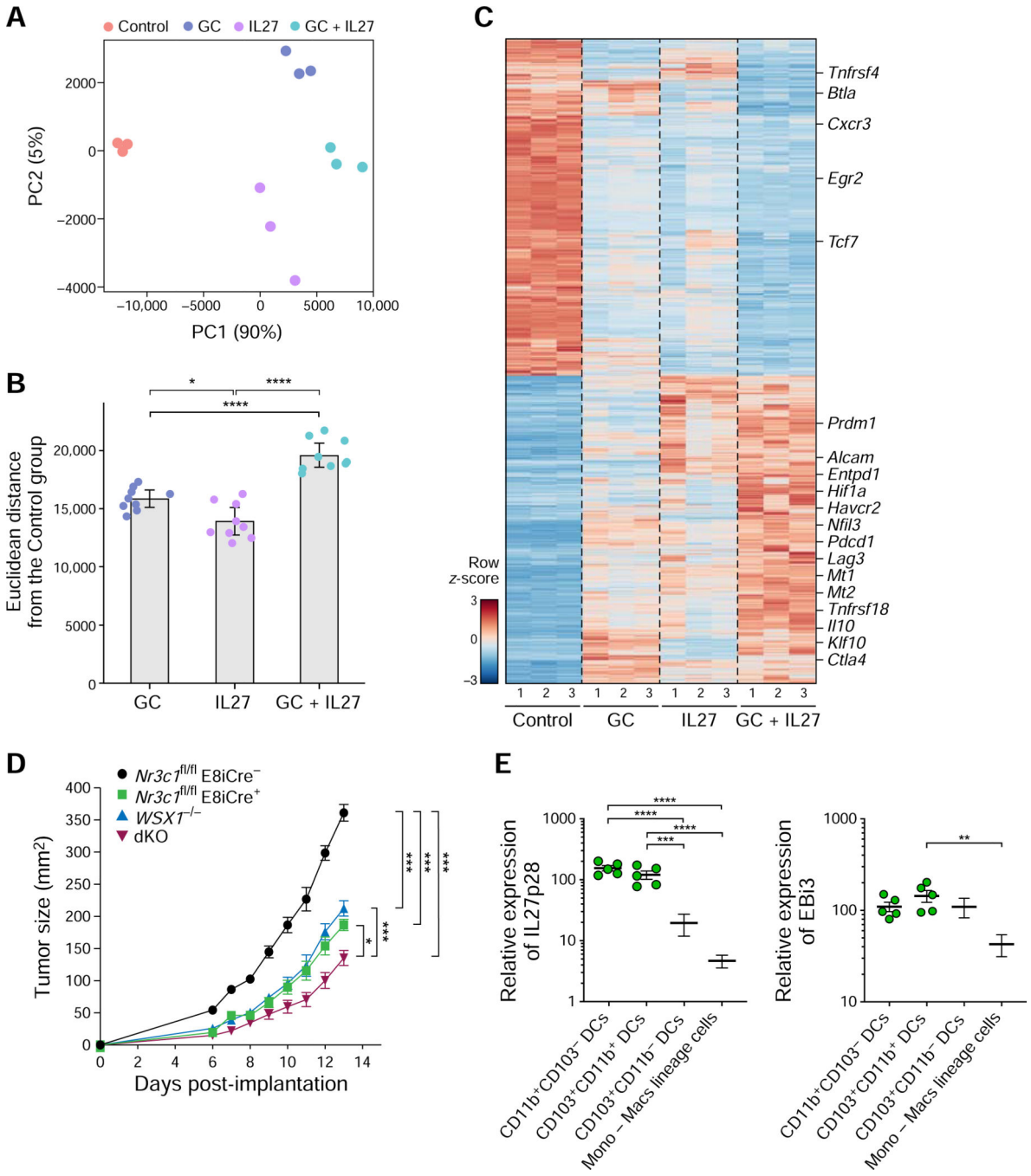

Figure 7: Glucocorticoid and IL-27 signaling co-operate to regulate CD8$^+$ T cell phenotype in the TME

A-C) Naïve CD8$^+$ T cells were cultured *in vitro* with anti CD3/28 and GC (dexamethasone), IL-27, or GC+IL-27. Cells were harvested on Day 9 and gene expression analyzed by RNA sequencing.

A) Principle component analysis (PCA) of Ctrl, GC, IL-27, and GC+IL-27 treated CD8$^+$ T cells. The percentage of explained variance for each principal component is indicated.

B) Mean delta Euclidean distance between the GC, IL-27, or GC+IL-27-treated groups to thecontrol group, adjusted p-values were calculated using one-way ANOVA ($p=9.89\times10^{-09}$), followed by Tukey's multiple comparisons test, *p<0.05, ****p<0.001.
C) Heatmap of DE genes between Ctrl and GC + IL-27 treatment. Tick marks indicateselected genes associated with $CD8^+$ T cell dysfunction.
D) $CD8^+$ T cells from either WT (E8i-Cre^-*Nr3c1*$^{fl/fl}$), E8i-Cre^+*Nr3c1*$^{fl/fl}$, $WSX1^{-/-}$ or and E8i-Cre^+*Nr3c1*$^{fl/fl}$ $WSX1^{-/-}$ (DKO) mice and $CD4^+$ T cells from WT mice were transferred to $Rag^{-/-}$mice (n=5–6/group), MC38-Ova^{dim} cells were implanted two days post T cell transfer. Mean tumor growth is shown. *p<0.05, ***p< 0.001, linear mixed model. Data are representative of 2 independent experiments.
E) qRT-PCR analysis of IL-27 (p28 and Ebi3) mRNA expression in the indicated cells. Dataare pooled from 2 independent experiments. **p<0.01, ***p<0.001, ****p<0.0001. One-way ANOVA (Tukey's multiple comparisons test). Data are mean ± SEM.

KEY RESOURCES TABLE

REAGENT or RESOURCE	SOURCE	IDENTIFIER
Antibodies		
Anti-Mouse CD4 RM4–5 APC/Cy7	Biolegend	Cat:# 100526
Anti-Mouse CD4 RM4–5 BV421	Biolegend	Cat:# 100563
Anti-Mouse CD8a 53–6.7 APC/Cy7	Biolegend	Cat:# 100714
Anti-Mouse CD8a 53–6.7 BV421 100753	Biolegend	Cat:# 100738
Anti-Mouse Tim-3 5D12 APC	Biolegend	custom order
Anti-Mouse PD-1 RMP1–30 PE/Cy7	Biolegend	Cat:# 109110
Anti-Mouse TIGIT GIGD7 PerCP-eFluor710	Thermo Fisher	Cat:# 46–9501-82
Anti-Mouse Lag-3 C9B7W PE	Thermo Fisher	Cat:# 12–2231-83
Anti-Mouse GR G-5 PE	Santa Cruz Biotechnology	Cat:# sc-393232
Anti-Mouse CD107a 1D4B APC	Biolegend	Cat:# 121614
Anti-Mouse Granzyme B NGZB FITC	Thermo Fisher	Cat:# 11–8898-82
Anti-Mouse IL-10 JES5–16E3 APC	Biolegend	Cat:# 505010
Anti-Mouse IL-10 JES5–16E3 BV605	Biolegend	Cat:# 505031
Anti-Mouse IL-2 JES6–5H4 PE	Biolegend	Cat:# 503808
Anti-Mouse IFNγ XMG1.2 APC/Cy7	Biolegend	Cat:# 505850
Anti-Mouse TNFα MP6-XT22 FITC	Biolegend	Cat:# 506304
Anti-Mouse TNFα MP6-XT22 PE/Cy7	Biolegend	Cat:# 506324
Anti-Mouse CD45 30-F11 AF700	Biolegend	Cat:# 103128
Anti-Mouse CD45.1 A20 APC-Cy7	Biolegend	Cat:# 110716
Anti-Mouse CD45.2 104 FITC	Biolegend	Cat:# 109806
Anti-Mouse CD3 145–2C11 PE	Biolegend	Cat:# 100308
Anti-Mouse CD19 6D5 PE	Biolegend	Cat:# 115508
Anti-Mouse NK1.1 PK136 PE	Biolegend	Cat:# 108708
Anti-Mouse Ly-6C HK1.4 PE	Biolegend	Cat:# 128008
Anti-Mouse Ly-6G 1A8 PE	Biolegend	Cat:# 127607
Anti-Mouse Siglec-F E50–2440 PE	BD Biosciences	Cat:# 552126
Anti-Mouse CD11b M1/70 BV421	Biolegend	Cat:# 101236
Anti-Mouse CD11c N418 PerCP/Cy5.5	Biolegend	Cat:# 117328
Anti-Mouse CD24 M1/69 APC	Biolegend	Cat:# 101814
Anti-Mouse I-A/I-E M5/114.15.2 FITC	Biolegend	Cat:# 107606
Anti-Mouse F4/80 BM8 PE	Biolegend	Cat:# 123110
Anti-Mouse CD103 2E7 PE/Cy7	Biolegend	Cat:# 121426
Anti-Human CD3 UCHT1 AF700	Biolegend	Cat:# 300424
Anti-Human CD8a RPA-T8 FITC	Biolegend	Cat:# 301060
Anti-Human CD8a RPA-T8 PerCP/Cy5.5	Biolegend	Cat:# 301032
Anti-Human Tim-3 F38–2E2 BV421	Biolegend	Cat:# 345008

REAGENT or RESOURCE	SOURCE	IDENTIFIER
Anti-Human PD-1 EH12.2H7 APC/Fire750	Biolegend	Cat:# 329954
Anti-Human CCR7 G043H7 PE	Biolegend	Cat:# 353204
Anti-Human CD62L DREG56 APC	Biolegend	Cat:# 304810
Anti-Human CD45RA HI 100 FITC	Biolegend	Cat:# 304106
Anti-Human PD-1 EH12.2H7 PE/Cy7	Biolegend	Cat:# 329918
Anti-Human TIGIT MBSA43 PE	Thermo Fisher	Cat:# 12–9500-42
Anti-Human Lag-3 11C3C65 AF647	Biolegend	Cat:# 369304
Bacterial and Virus Strains		
Biological Samples		
Chemicals, Peptides, and Recombinant Proteins		
16% paraformaldehyde	Electron Microscopy Sciences	
DMEM	GIBCO	Cat#:11–965-118
M199 Hank's Balanced Salts	GIBCO	Cat#:12–350-039
NEEA	GIBCO	Cat:# 11140050
NaPyruvate	GIBCO	Cat:# 11360070
Fetal Bovine Serum	SIGMA	Cat:# F2442
Collagenase IV	Gibco	Cat:# 17104019
Percoll	GE Healthcare	Cat:# 17089101
Golgi Stop	BD Biosciences	Cat:# 554724
Golgi Plug	BD Biosciences	Cat:# 555029
$OVA_{257–264}$ peptide	AnaSpec	Cat:# AS-60193–5
CountBright™ Absolute Counting Beads	Thermo Fisher	Cat:# C36950
Zombie UV fixable viability dye	Biolegend	Cat:# 423108
Fixable viability dye eF506	Thermo Fisher	Cat:# 65–0866-14
RLT Plus lysis buffer	Qiagen	Cat:#1053393
SuperScript™ IV VILO™ Master Mix	Thermo Fisher Scientific	Cat:# 11756500
PicoPure™ RNA Isolation Kit	Thermo Fisher Scientific	Cat:# KIT0204
RNeasy Plus Mini Kit	Qiagen	Cat:# 74134
Dexamethosone	Sigma-Aldrich	Cat:# D4902–25MG
Corticosterone	Fischer Scientific	Cat:# 368550R
Metyrapone	Fischer Scientific	Cat:# 329250
Acetonitrile	Sigma-Aldrich	Cat:# 360457
Hexane	Sigma-Aldrich	Cat:# 32293
Recombinant Mouse IL27	R&D Systems	Cat:# 2799-ML-010
Critical Commercial Assays		
FoxP3 Transcription Factor Staining Buffer Set	eBioscience	Cat:# 00–5523-00
Corticosterone ELISA Kit	Arbor Assays	Cat:# K014-H1

REAGENT or RESOURCE	SOURCE	IDENTIFIER
Pregnenolone ELISA Kit	Abnova	Cat:# KA1912
BD Cytofix/Cytoperm™	BD Biosciences	Cat # 554714
NextSeq 500/550 High Output v2 kit (75 cycles)	Illumina	Cat# FC-404–2005
Nextera XT DNA Library Preparation Kit	Illumina	Cat# FC-131–1024
Dual-Luciferase® Reporter Assay System	Promega	Cat:# E1910
Deposited Data		
Sequence data	This paper	GEO: GSE153556
Experimental Models: Cell Lines		
B16F10 melanoma	ATCC	#CRL-6475
MC38 colon carcinoma	Laboratory of Dr. Mark Smyth	
MC38-OVA colon carcinoma	Laboratory of Dr. Mark Smyth	
Cryopreserved sperm from males bearing a targeted Cyp11a1 allele	EUCOMM	
Experimental Models: Organisms/Strains		
C57BL/6 mice	Jackson laboratory	000664
C57BL/6 CD45.1 mice	Jackson laboratory	002014
Nr3c1 fl/fl mice	Jackson laboratory	021021
E8i-Cre mice	Jackson laboratory	008766
$Rag^{-/-}$ mice	Jackson Laboratory	002216
LysMCre mice	Jackson laboratory	004781
WSX1−/− mice	Jackson laboratory	018078
Cyp11a1fl/fl	This paper	N/A
Oligonucleotides		
Cyp11a1 (Mm00490735_m1)	Thermo Fischer Scientific	Cat# 4331182
StAR (Mm00441558_m1)	Thermo Fischer Scientific	Cat# 4331182
Hsd3b1 (Mm01261921_mH)	Thermo Fischer Scientific	Cat# 4351372
Cyp17a1 (Mm00484040_m1)	Thermo Fischer Scientific	Cat# 4331182
Cyp21a1 (Mm00487230_g1)	Thermo Fischer Scientific	Cat# 4331182
Hsd3b3 (Mm05682013_s1)	Thermo Fischer Scientific	Cat# 4351372
Hsd3b6 (Mm00834440_m1)	Thermo Fischer Scientific	Cat# 4331182
Cyp11b1 (Mm01204952_m1)	Thermo Fischer Scientific	Cat# 4331182
IL27p28 (Mm00461162_m1)	Thermo Fischer Scientific	Cat# 4331182
Ebi3 (Mm00469294_m1)	Thermo Fischer Scientific	Cat# 4331182
Beta-Actin (Mm02619580_g1)	Thermo Fischer Scientific	Cat# 4448489
Recombinant DNA		
pGL4.10 Luciferase reporter plasmid	Promega	Cat# E6651
pGL4.23 Luciferase reporter plasmid	Promega	Cat# E8411
Nr3c1 cDNA ORF clone in pcDNA3.1+ vector	GeneScript	Cat# NM_008173.3

REAGENT or RESOURCE	SOURCE	IDENTIFIER
Software and Algorithms		
FlowJo software	Tree Star	https://flowjo.com
Prism 8	GraphPad Software, Inc	https://www.graphpad.com/
t-SNE R implementation	Maaten, 2009; Maaten L, 2008	https://github.com/jdonaldson/rtsne/
Bioconductor package DESeq in R	Anders and Huber, 2010	